DIFFUSION MODELS DO NOT IMPLICITLY LEARN CONDITIONAL INDEPENDENCE

Sachit Gaudi **Gautam Sreekumar** **Vishnu Naresh Boddeti**
Michigan State University
{gaudisac,sreekum1,vishnu}@msu.edu

ABSTRACT

How can we learn generative models to sample data with arbitrary logical compositions of statistically independent attributes? The prevailing solution is to sample from distributions expressed as a composition of attributes' *conditional marginal distributions* under the assumption that they are statistically independent. This paper shows that standard conditional diffusion models violate this assumption, even when all attribute compositions are observed during training. And, this violation is significantly more severe when only a subset of the compositions is observed. We propose COIND to address this problem. It explicitly enforces statistical independence between the *conditional marginal distributions* by minimizing Fisher's divergence between the *joint* and *marginal* distributions. The theoretical advantages of COIND are reflected in both qualitative and quantitative experiments, demonstrating a significantly more faithful and controlled generation of samples for arbitrary logical compositions of attributes. The benefit is more pronounced for scenarios that current solutions relying on the assumption of *conditionally independent marginals* struggle with, namely, logical compositions involving the NOT operation and when only a subset of compositions are observed during training. Our code is available at https://github.com/sachit3022/compositional-generation/

1 INTRODUCTION

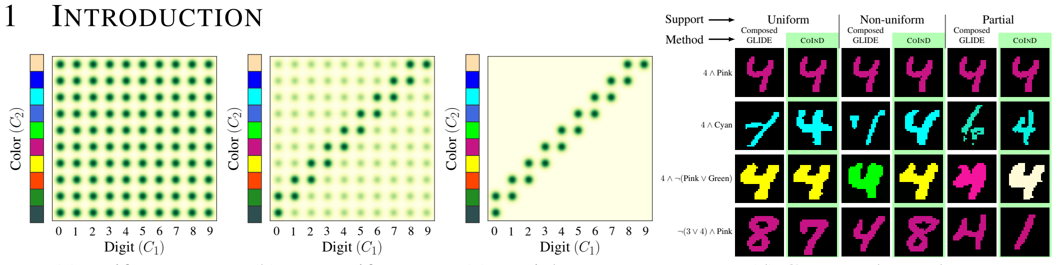

(a) Uniform (b) Non-uniform (c) Partial support (d) Generated samples

Figure 1: **Generative Modeling of Logical Compositions.** (a-c) Consider the task of generating MNIST samples for any logical composition of digits and colors by learning on observational data of different supports. (d) Standard diffusion models fail to generate data with arbitrary logical compositions of attributes. We generate data from simple unseen compositions (row 2), and more complex logical compositions (rows 3,4) through COIND, even under non-uniform and partial support.

Many applications of generative models, including image editing (Kim et al., 2022; Brooks et al., 2022), desire explicit and independent control over statistically independent attributes. For example, in face generation, one might want to control the amount of hair, smile, etc., independently. Consider the illustrative task in Fig. 1 of generating realistic samples of colored handwritten digits with explicit and independent control over the composition of color and digit. For example, "generate an image of digit 4 while excluding the colors green and pink". This composition can be logically expressed as "$4 \wedge \neg$[Green$\vee$Pink]", where $\wedge$, $\vee$, and $\neg$ represent the three primitive logical operators AND, OR, and NOT, respectively.

Existing solutions (Liu et al., 2023; Du et al., 2020; Nie et al., 2021) realize this goal by mapping the logical expressions into a probability distribution involving the conditional marginal distributions

$p(\text{image} \mid \text{digit} = 4)$, $p(\text{image} \mid \text{color} \neq \text{Green})$, and $p(\text{image} \mid \text{color} \neq \text{Pink})$, and sampling from it. These marginal distributions are obtained either by learning separate energy-based models for each compositional attribute (Du et al., 2020; Nie et al., 2021) or by factorizing the attributes' learned joint distribution Liu et al. (2023). Both approaches, however, are predicated on the critical assumption that the conditional marginal distributions are statistically independent of each other.

Employing the approaches mentioned above, for instance Liu et al. (2023), to our illustrative example, we observe that when the conditional diffusion model is learned on data with non-uniform (Fig. 1b) or partial (Fig. 1c) support of the compositional attributes, the models fail to generate realistic samples (columns 3 and 5 of row 2 in Fig. 1d) or generate realistic samples with logically inaccurate compositions (columns 3 and 5 of rows 3 and 4 in Fig. 1d). This is true even for simple unseen logical compositions of attributes (AND in row 2 of Fig. 1d) or for complex logical compositions (rows 3 and 4 of Fig. 1d involving a NOT operation). Such failure under partial support was also observed by Du et al. (2020). Surprisingly, note that even when all compositions of the attributes are observed, the model fails to generate realistic samples (column 1 of row 2 in Fig. 1d).

These observations naturally raise the following research questions that this paper seeks to answer:

– (RQ1) *Why do standard classifier-free conditional diffusion models fail to generate data with arbitrary logical compositions of attributes?* We hypothesize that violating the assumption that the conditional marginal distributions are statistically independent of each other will result in poor image quality, diminished control over the generated image attributes, and, ultimately, failure to adhere to the desired logical composition. We verify and confirm our hypothesis through a case study in § 3.

– (RQ2) *How can we explicitly enable conditional diffusion models to generate data with arbitrary logical compositions of attributes?* We adopt the principle of independent causal mechanisms (Peters et al., 2017) to express the conditional data likelihood in terms of the constituent conditional marginal distributions to ensure that the model does not learn non-existent statistical dependencies from the training data.

Summary of contributions.

1. In Section 3, we show that conditional diffusion models trained to maximize the likelihood of the observed data do not learn independent conditional marginal distributions. Instead, the models learn non-existent statistical dependencies induced by unknown confounding factors.
2. Through causal modeling, we derive a training objective, COIND, comprising the standard score-matching loss and a conditional independence violation loss required to enforce the conditional independence relations necessary for enabling logical compositions in conditional diffusion models.
3. Strong inductive biases, in the form of the conditional independence relations in COIND, enable arbitrary logical compositionality in conditional diffusion models with fine-grained control over conditioned attributes and diversity for unconditioned attributes. COIND achieves these goals while being monolithic and is scalable with the number of attributes.

2 Logical Compositionality in Diffusion Models

We study the problem of generating data with attributes that satisfy a given logical relation between them. We consider the case where the attributes are statistically independent of each other. However, not all attribute compositions may be observed during training. To study this problem, we first model the underlying data-generation process using a suitable causal model that relates data and their independently varying attributes.

Notations. We use bold lowercase and uppercase characters to denote vectors (e.g., $\boldsymbol{a}$) and matrices (e.g., $\boldsymbol{A}$) respectively. Random variables are denoted by uppercase Latin characters (e.g., X). The distribution of a random variable X is denoted as $p(X)$, or as $p_{\boldsymbol{\theta}}(X)$ if the distribution is parameterized by a vector $\boldsymbol{\theta}$. We adopt non-standard terminology where *marginals* denote the conditionals $p(\mathbf{X} \mid C_i)$ rather than integrated marginals, $p(C_i)$ emphasizing their functional role as modular components in our compositional framework. Correspondingly, *joint* refers to $p(\mathbf{X} \mid C)$, acknowledging this deliberate departure from probabilistic conventions due to a lack of better terminology.

Data Generation Process. The data generation process consists of observed data $\boldsymbol{X}$ (e.g., images) and its attribute variables $C_1, C_2, \ldots, C_n$ (e.g., color, digit, etc.). To have explicit control over these attributes during generation, they should vary independently of each other. In this work, we limit our study to only those causal graphs in which the attributes are not causally related and can hence vary independently, as shown in Fig. 2a. Each C_i assumes values from a set $\mathcal{C}_i$ and their Cartesian product $\mathcal{C} = \mathcal{C}_1 \times \cdots \times \mathcal{C}_n$ is referred to as the *attribute space*. Each attribute C_i generates its own observed component $\boldsymbol{X}_{C_i} = f_{C_i}(C_i)$, which together with unobserved exogenous variables $\boldsymbol{U}_{\boldsymbol{X}}$ form the composite observed data $\boldsymbol{X} = f(\boldsymbol{X}_{C_1}, \ldots, \boldsymbol{X}_{C_i}, \boldsymbol{U}_{\boldsymbol{X}})$ (see Fig. 2a). We do not restrict f much except that it should not obfuscate individual observed components in $\boldsymbol{X}$ (Wiedemer et al., 2024). A simple example of f is the concatenation function. We also assume that all f_{C_i} are invertible and therefore it is possible to estimate $C_1, \ldots, C_n$ from $\boldsymbol{X}$. These assumptions together ensure that $C_1, \ldots, C_n$ are mutually independent given $\boldsymbol{X}$ despite being seemingly d-connected.

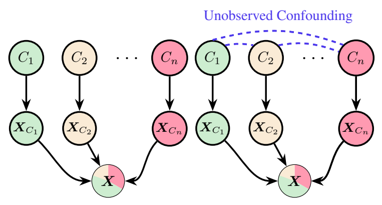

(a) True underlying causal model (b) Causal model during training

Figure 2: (a) $C_1, C_2, \ldots, C_n$ vary freely and independently in the underlying causal graph. (b) However, they become dependent during training due to unknown and unobserved confounding factors.

Problem Statement. When the training data is sampled according to the causal graph in Fig. 2a, all attribute compositions are equally likely to be observed. We refer to this scenario as *uniform support*. Although the attributes can vary independently, sometimes they may not do so in the training dataset due to unobserved confounding such as sample selection bias (Storkey, 2008), leading to an *attribute shift*. In such cases, the underlying causal model during training modifies as shown in Fig. 2b, where blue dashed curves denote the unobserved confounding. In practice, all attribute compositions may be observed with unequal probabilities. We refer to this scenario as *non-uniform support*. In some cases, this dependence could lead to the training samples consisting of only a subset of all attribute compositions as shown in Fig. 1c, i.e., $\mathcal{C}_{\text{train}} \subset \mathcal{C}$. We refer to this scenario as *partial support*. We aim to learn conditional diffusion models under these scenarios to generate samples with attributes that satisfy a given logical compositional relation between them.

The attribute space in our problem statement has the following properties. **(1)** Every possible value that C_i can assume is present in the training set, and open-set attribute compositions do not fall under this definition. **(2)** For every ordered tuple $c \in \mathcal{C}_{\text{train}}$, there is another $c' \in \mathcal{C}_{\text{train}}$ such that c and c' differ on only one attribute. Similar assumptions were discussed in (Wiedemer et al., 2024).

Preliminaries on Score-based Models. In this work, we train conditional score-based models (Song et al., 2021) using classifier-free guidance (Ho & Salimans, 2022) to generate data corresponding to a given logical attribute composition. Score-based models learn the score of the observed data distributions $p_{\text{train}}(\boldsymbol{X})$ and $p_{\text{train}}(\boldsymbol{X} \mid C)$ through score matching (Hyvärinen & Dayan, 2005). Once the score of a distribution is learned, samples can be generated using Langevin dynamics. For logical attribute compositional generation, the given attribute composition is decomposed in terms of two primitive logical compositions: (1) AND operation (e.g., $C_1 = c_1 \wedge C_2 = c_2$ generates data where attributes C_1 and C_2 takes values c_1 and c_2 respectively), and (2) NOT operation (e.g., $C_1 = \neg c_1$ generates data where the attribute C_1 takes any value except c_1). Liu et al. (2023) proposed the following modifications during sampling to enable AND and NOT logical operations between the attributes, assuming that the diffusion model learns the conditional independence relations from the underlying data-generation process, i.e., $p(C_1, \ldots, C_n|\boldsymbol{X}) = \prod_{i=1}^{n} p(C_i|\boldsymbol{X})$.

Logical AND ($\wedge$) operation: Since $p_{\boldsymbol{\theta}}(C_1 \wedge C_2 \mid \boldsymbol{X}) = p_{\boldsymbol{\theta}}(C_1 \mid \boldsymbol{X}) p_{\boldsymbol{\theta}}(C_2 \mid \boldsymbol{X})$ samples are generated for the logical composition $C_1 \wedge C_2$ by sampling from the following score:

$$\nabla_{\boldsymbol{X}} \log p_{\boldsymbol{\theta}}(\boldsymbol{X} \mid C_1 \wedge C_2) = \nabla_{\boldsymbol{X}} \log p_{\boldsymbol{\theta}}(\boldsymbol{X} \mid C_1) + \nabla_{\boldsymbol{X}} \log p_{\boldsymbol{\theta}}(\boldsymbol{X} \mid C_2) - \nabla_{\boldsymbol{X}} \log p_{\boldsymbol{\theta}}(\boldsymbol{X}) \quad (1)$$

Logical NOT ($\neg$) operation: Following the approximation $p_{\boldsymbol{\theta}}(\neg C_2 \mid \boldsymbol{X}) \propto \frac{1}{p_{\boldsymbol{\theta}}(C_2|\boldsymbol{X})}$, the score to sample data for the logical composition $C_1 \wedge \neg C_2$ can be expressed as,

$$\nabla_{\boldsymbol{X}} \log p_{\boldsymbol{\theta}}(\boldsymbol{X} \mid C_1 \wedge \neg C_2) = \nabla_{\boldsymbol{X}} \log p_{\boldsymbol{\theta}}(\boldsymbol{X}) + \nabla_{\mathbf{X}} \log p_{\boldsymbol{\theta}}(\boldsymbol{X} \mid C_1) - \nabla_{\mathbf{X}} \log p_{\boldsymbol{\theta}}(\boldsymbol{X} \mid C_2) \quad (2)$$

Note that the scores to sample from these primitive logical compositions involve conditional *marginal* likelihood terms $\boldsymbol{X} \mid C_i$. Therefore, to perform logical composition, it is critical to accurately learn the conditional *marginals* of the attributes.

Evaluation We evaluate the distributions learned by the model based on their accuracy in generating images with attributes that align with the desired compositions for a logical relation. For example, to evaluate AND ($\wedge$) composition, consider sampling an arbitrary digit and color, represented as $C = (4, \text{Cyan})$. We generate images $\hat{X}$ by sampling from Eq. (1), and subsequently infer attributes, $(\hat{c}_1, \hat{c}_2) = (\phi_{C_1}(\hat{X}), \phi_{C_2}(\hat{X}))$. We then verify if $(\hat{c}_1, \hat{c}_2) \subseteq \{4\} \times \{\text{Cyan}\}$, and this process is averaged over all combinations in $\mathcal{C}$ to obtain CS. Further details regarding the Conformity Score including the formal definition can be found in App. D.6.

3 Why do conditional diffusion models fail to generate data with arbitrary logical compositions of attributes?

To address **(RQ1)**, we utilize the task of generating synthetic images from the Colored MNIST dataset for *any* given combination of color and digit, as introduced in § 1. However, not all the desired compositions may be observed during training. To study the effect of data support, we consider the three training distributions of attribute compositions defined in § 2: (1) uniform support (Fig. 1a), (2) non-uniform support (Fig. 1b), and (3) partial support (Fig. 1c). To quantify the dependence in the observational data we measure Mutual Information (MI) between attributes. Refer to App. D.4 for visual representation and exact formulation.

For each support, we train a diffusion model and evaluate the conditional *joint*, $p_{\boldsymbol{\theta}}(X \mid C)$ and *marginal*, $p_{\boldsymbol{\theta}}(X \mid C_i)$ distributions. During inference, the images are separately sampled from the *joint* distribution, $\nabla_{\boldsymbol{X}} \log p_\theta(\boldsymbol{X} \mid C)$, and from the product of the learned *marginals* as shown in Eq. (1). We refer to the former method as *joint sampling* and the latter as *marginal* sampling. To measure the accuracy of the attributes in the generated image in accordance to the desired attributes, we use conformity score (CS) defined in § 2. Tab. 1 compares the *joint* and the *marginal* distributions learned by models trained under various training scenarios. We draw the following conclusions.

Support (MI)	Conformity Score		JSD ↓
	Joint ↑	*Marginal* ↑	
Uniform (0.00)	99.98	98.15	0.16
Non Uniform (0.33)	99.98	86.10	0.30
Partial (1.70)	33.14	7.40	2.75

Table 1: **Conformity Scores** and **Jensen-Shannon divergence** for samples generated from joint and marginal distributions learned by models under various support settings for the Colored MNIST dataset.

Diffusion models struggle to generate unseen attribute compositions. Conformity scores from joint sampling Tab. 1 reveals that while models trained with uniform and non-uniform support accurately generate samples with correct attribute compositions, those trained with partial support struggle with unseen attribute compositions. This phenomenon stems from the diffusion models' objective of maximizing conditional generation likelihood. With full support, models accurately learn $p_{\boldsymbol{\theta}}(\boldsymbol{X} \mid C) \approx p_{\text{train}}(\boldsymbol{X} \mid C)$. However, partial support leads to inaccurate density learning in unobserved regions, as the model does not encounter samples for every attribute composition from $p_{\text{train}}(\boldsymbol{X} \mid C)$. Conformity scores further decrease when sampling from the product of marginals. This discrepancy in CS, when sampled from joint and product of marginals is due to violation of conditional independence Refer App. B.1 for detailed proof.

We measure CI violation as the disparity between the conditional joint distribution $p_{\boldsymbol{\theta}}(C \mid \boldsymbol{X})$ and the product of conditional marginal distributions $\prod_i^n p_{\boldsymbol{\theta}}(C_i \mid \boldsymbol{X})$ learned by the implicit classifier of diffusion model using Jensen-Shannon divergence (JSD). Note that JSD, measure *conditional* independence, whereas MI measure independence between attributes. More details in App. D.7.

Diffusion models violate conditional independence assumption. A positive JSD value suggests that the model fails to adhere to the independence relations present in the underlying causal model. Our findings in Tab. 1 indicate that as the training distribution of attribute compositions diverges from the true underlying distribution – where attributes can vary independently – the trained models increasingly violate these independence relations, as reflected by the JSD measurements.

Violation in conditional independence originates from the standard training objective of diffusion models that maximize the likelihood of conditional generation. Under perfect loss, for every observed composition ($C \in \mathcal{C}_{train}$), the model accurately learns $p_{\text{train}}(\boldsymbol{X} \mid C)$, i.e., $p_{\boldsymbol{\theta}}(\boldsymbol{X} \mid C) \approx p_{\text{train}}(\boldsymbol{X} \mid C) = p(\boldsymbol{X} \mid C)$, However, learn incorrect marginals, $p_{\boldsymbol{\theta}}(\boldsymbol{X} \mid C_i) \approx p_{\text{train}}(\boldsymbol{X} \mid C_i) \neq p(\boldsymbol{X} \mid C_i)$. Refer to App. B.2 for complete proof. These incorrect marginals lead to violation in CI.

Diffusion models learn the dependence in the underlying distribution. The violation of conditional independence strongly correlates with the mutual information (MI) between attributes in training data Pearson's $r = 0.999, p < 0.03$. These findings Tab. 1 demonstrate diffusion models lack inherent compositional bias, instead propagate dependencies as present in their training data.

Based on these observations, we propose COIND to train diffusion models that explicitly enforce the conditional independence dictated by the underlying causal data-generation process to encourage the model to learn accurate marginal distributions of the attributes.

4 COIND: ENFORCING CONDITIONALLY INDEPENDENT MARGINAL TO ENABLE LOGICAL COMPOSITIONALITY

In this section, we propose COIND to answer **(RQ2)** posed in § 1: *How can we explicitly enable conditional diffusion models to generate data with arbitrary logical compositions of attributes?*

In the previous section, we observed that diffusion models do not obey the underlying causal relations, learning incorrect attribute *marginals*, and hence struggling to demonstrate logical compositionally as we showed in Fig. 1. To remedy this, COIND uses a training objective that explicitly enforces the causal factorization to ensure that the trained diffusion models obey the underlying causal relations. From the causal graph Fig. 2a, along with the assumption of $C_1 \perp\!\!\!\perp \ldots \perp\!\!\!\perp C_n \mid \boldsymbol{X}$ mentioned in § 2, we have $p(\boldsymbol{X} \mid C) = \frac{p(\boldsymbol{X})}{p(C)} \prod_i^n \frac{p(\boldsymbol{X}|C_i)p(C_i)}{p(\boldsymbol{X})}$. Note that the invariant $p(\boldsymbol{X} \mid C)$ is now expressed as the product of *marginals* employed for sampling. Therefore, training the diffusion model by maximizing this conditional likelihood is naturally more suited for learning accurate *marginals* for the attributes. We minimize the distance between the true conditional likelihood and the learned conditional likelihood as,

$$\mathcal{L}_{\text{comp}} = \mathcal{W}_2 \left(p(\boldsymbol{X} \mid C), \frac{p_{\boldsymbol{\theta}}(\boldsymbol{X})}{p_{\boldsymbol{\theta}}(C)} \prod_i \frac{p_{\boldsymbol{\theta}}(\boldsymbol{X} \mid C_i) p_{\boldsymbol{\theta}}(C_i)}{p_{\boldsymbol{\theta}}(\boldsymbol{X})} \right) \tag{3}$$

By applying the triangle inequality and leveraging the Wasserstein distance upper bound via Fisher divergence (Kwon et al., 2022), we derive the following inequality:

$$\mathcal{L}_{\text{comp}} \leq K_1 \sqrt{\mathcal{L}_{\text{score}}} + K_2 \sqrt{\mathcal{L}_{\text{CI}}} \tag{4}$$

for constants $K_1, K_2 > 0$. A complete derivation of this bound is provided in App. B.3.

Distribution matching:

$$\mathcal{L}_{\text{score}} = \mathbb{E}_{p(\boldsymbol{X},C)} \|\nabla_{\boldsymbol{X}} \log p_{\boldsymbol{\theta}}(\boldsymbol{X} \mid C) - \nabla_{\boldsymbol{X}} \log p(\boldsymbol{X} \mid C)\|_2^2 \tag{5}$$

Conditional Independence:

$$\mathcal{L}_{\text{CI}} = \mathbb{E} \|\nabla_{\mathbf{X}} \log p_\theta(\mathbf{X} \mid C) - \nabla_{\mathbf{X}} \log p_\theta(\mathbf{X}) - \sum_i \left[\nabla_{\mathbf{X}} \log p_\theta(\mathbf{X} \mid C_i) - \nabla_{\mathbf{X}} \log p_\theta(\mathbf{X})\right] \|_2^2 \tag{6}$$

Practical Implementation. A computational burden presented by $\mathcal{L}_{\text{CI}}$ in Eq. (6) is that the required number of model evaluations increases linearly with the number of attributes. To mitigate this burden, we approximate the mutual conditional independence with pairwise conditional independence (Hammond & Sun, 2006). Thus, the modified $\mathcal{L}_{\text{CI}}$ becomes,

$$\mathcal{L}_{\text{CI}} = \mathbb{E}_{p(\boldsymbol{X},C)} \mathbb{E}_{j,k} \|\nabla_{\boldsymbol{X}} \log p_\theta(\boldsymbol{X} \mid C_j, C_k) - \nabla_{\boldsymbol{X}} \log p_\theta(\boldsymbol{X} \mid C_j) - \nabla_{\boldsymbol{X}} \log p_\theta(\boldsymbol{X} \mid C_k) + \nabla_{\boldsymbol{X}} \log p_\theta(\boldsymbol{X})\|_2^2$$

The weighted sum of the square of the terms in Eq. (4) has shown stability. Therefore, COIND's training objective:

$$\mathcal{L}_{\text{final}} = \mathcal{L}_{\text{score}} + \lambda \mathcal{L}_{\text{CI}} \tag{7}$$

where λ is the hyper-parameter that controls the strength of conditional independence. The reduction to the practical version of the upper bound (Eq. (4)) is discussed in extensively in App. C. For guidance on selecting hyper-parameters in a principled manner, please refer to App. C.3. Finally, our proposed approach can be implemented with just a few lines of code, as outlined in Algorithm 1.

5 Experiments: Learning Independent Marginals Enables Logical Compositionality

CoInD encourages diffusion models to learn conditionally independent marginals of attributes, and thereby improve their logical compositionality capabilities. In this section, we design experiments to evaluate CoInD on two questions: (1) *does* CoInD *effectively train diffusion models that obey the underlying causal model?*, and (2) *does* CoInD *improve the logical compositionality of these models?* We measure the JSD of the trained models to answer the first question. To answer the second question, we use two primitive logical compositional tasks: (a) $\wedge$ (AND) composition and (b) $\neg$ (NOT) composition. In each case, the generative model is provided with a logical relation between the attributes, and the task is to generate images with attributes that satisfy this logical relation. A more detailed description of task construction can be found in App. D.2.

Datasets. We use the following image datasets with labeled attributes for our experiments: **(1) Colored MNIST** dataset described in § 1, where the attributes of interest are digit and color, **(2) Shapes3d** dataset (Burgess & Kim, 2018) containing images of 3D objects in various environments where each image is labeled with six attributes of interest. Refer to App. D.5 for details.

Observed training distributions. We evaluate CoInD on four scenarios where we observe different distributions of attribute compositions during training: (1) Uniform support (Fig. 1a). (2) Non-uniform support (Fig. 1b), (3) Diagonal partial support (Fig. 1c), and (4) Orthogonal partial support. includes only the attribute compositions along the axes originating from a corner of the hypercube $\mathcal{C}$, following (Wiedemer et al., 2024).

Baselines. **LACE** (Nie et al., 2021) and **Composed GLIDE** (Liu et al., 2023) are our primary baselines. LACE trains distinct energy-based models (EBMs) for each attribute and combines them following the compositional logic described in § 2 during sampling. A similar approach was proposed by (Du et al., 2020). However, in our experimental evaluation for LACE, we train distinct score-based models instead of EBMs. In contrast, Composed GLIDE samples from score-based models by factorizing the joint distribution into marginals, assuming these models had implicitly learned conditionally independent marginals of attributes. Additional details about the baselines are delegated to App. D.3.

Metrics. We assess how accurately the models have captured the underlying data generation process using the JSD, defined in § 3. To measure the accuracy of the attributes in the generated image w.r.t. the input logical composition, we use conformity score (CS) from § 2. In addition to the conformity score, since the Shapes3d dataset contains unique ground truth images corresponding to the input logical relation, we directly compare generated samples with reference images, using variance-weighted R^2. For uniform and non-uniform support, the generations for the input logical relations correspond to attribute compositions that span the attribute space $\mathcal{C}$. In other cases, the generations for the input logical relations belong to the unseen compositional support, i.e., $\mathcal{C} \setminus \mathcal{C}_{\text{train}}$.

Support	Method	JSD ↓	$\wedge$ (CS) ↑	$\neg$ Color (CS)↑	$\neg$ Digit (CS) ↑
Uniform	LACE	-	96.40	92.56	83.67
	Composed GLIDE	0.16	98.15	99.30	81.64
	CoInD ($\lambda = 0.2$)	0.14	99.73	99.32	84.94
	CoInD ($\lambda = 1.0$)	**0.10**	**99.99**	**99.33**	**89.60**
Non-uniform	LACE	-	82.61	65.16	69.51
	Composed GLIDE	0.30	86.10	81.61	70.44
	CoInD ($\lambda = 1.0$)	**0.15**	**99.95**	**92.41**	**84.98**
Partial	LACE	-	10.85	9.03	28.24
	Composed GLIDE	2.75	7.40	5.09	33.86
	CoInD ($\lambda = 1.0$)	**1.17**	**52.38**	**53.28**	**52.59**

(a) Results on Colored MNIST Dataset

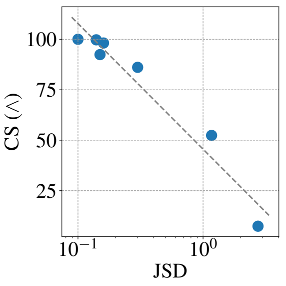

(b) JSD vs CS

Figure 3: **Results on Colored MNIST dataset.** (a) We compare JSD and CS of CoInD against baselines trained under various settings and on different compositional tasks. (b) Plotting CS against JSD in the log scale of the models trained under different settings reveals a negative correlation.

Table 3a compares CoInD against the baselines on $\wedge$ and $\neg$ composition tasks. "$\neg$ Color" task corresponds to image generation for a logical composition with $\neg$ operator acting on the color attribute. Similarly, the $\neg$ operator acts on the digit attribute in the "$\neg$ Digit" task. From the results, we make the following observations:

In practical scenarios of non-uniform and partial support, JSD increases with non-uniform support and worsens further with partial support due to incorrect marginals, as discussed in § 3. As such, we conjecture that scaling the datasets without inductive biases (conditional independence of marginals in this case) is insufficient for arbitrary logical compositional generation. Even methods like LACE, which train separate diffusion models for each attribute, fail. This suggests that softer inductive biases, such as learning separate marginals for each attribute without considering the desired independence relations, are insufficient for logical compositionality.

Logical AND ($\wedge$) and NOT ($\neg$) compositionality deteriorates as dependence between marginals increases. The negative correlation between JSD and CS, noted in § 3 and illustrated in Fig. 3b, is evident across different methods and observed support settings for $\wedge$ compositions. This strong negative correlation suggests that violations of conditional independence significantly impair the logical compositionality of standard diffusion models.

By enforcing conditional independence between the attributes during training, CoInD achieves lower JSD and improves both $\wedge$ and $\neg$ compositionality in non-uniform and partial support. The results in Fig. 3 demonstrate that **enforcing conditional independence between the marginals is vital for enabling arbitrary logical compositions in conditional diffusion models.**

CoInD generates diverse samples. It is desirable for generated samples to exhibit diverse values for attributes that are not explicitly controlled; otherwise, the model may reinforce undesirable stereotypes. Therefore, when conditioning on digit, CoInD generates diverse colors of samples, as quantified by the Shannon entropy Tab. 2. Unlike methods that explicitly optimize for diversity, CoInD achieves this as a complementary benefit by breaking dependencies induced by unknown confounders (see App. D.8 for details).

Method	**Entropy**
LACE	1.82
C GLIDE	1.71
CoInD	2.63

Table 2: Entropy of uncontrolled attribute in generation

Support	Method	JSD ↓	∧ Composition		¬ Composition	
			R^2 ↑	CS ↑	R^2↑	CS↑
Uniform	LACE	-	0.97	91.19	0.85	50.00
	Composed GLIDE	0.302	0.94	83.75	0.91	48.43
	CoInD ($\lambda = 1.0$)	**0.215**	**0.98**	**95.31**	**0.92**	**55.46**
Orthogonal	LACE	-	0.88	62.07	0.70	30.10
	Composed GLIDE	0.503	0.86	51.56	0.61	34.63
	CoInD ($\lambda = 1.0$)	**0.287**	**0.97**	**91.10**	**0.92**	**53.90**

(a) Results on Shapes3D Dataset

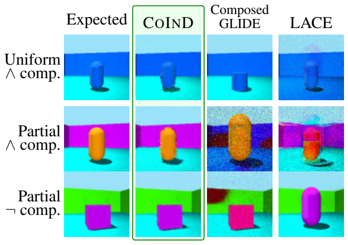

(b)

Figure 4: **Results on Shapes3d dataset.** (a) We compare JSD, R^2, and CS of CoInD against the baselines trained with uniform and partial support on the Shapes3d dataset for $\wedge$ and $\neg$ composition tasks. (b) Samples generated by CoInD match the expected image in all cases.

CoInD is scalable with attributes. Results on the Shapes3D (Table 4a) demonstrate that CoInD successfully composes even 6 attributes, showcasing strong compositional ability compared to baselines, specifically huge improvements on orthogonal support.

Generating Real-World Face Images using CoInD we evaluate CoInD on the CelebA dataset,

we evaluate CoInD on the CelebA dataset, generating face images with controlled ”smiling” and ”gender” attributes. To evaluate its capability on unseen compositions, we sample the training data such that the model does not observe any “male smiling” celebrities, equivalent to the orthogonal support.

Method	JSD ↓	“smiling male”		“smiling”∧“male”	
		CS ↑	FID ↓	CS ↑	FID ↓
LACE	-	-	-	**24.20**	80.40
Composed GLIDE	2.44	2.51	61.21	10.55	95.41
CoInD ($\lambda = 100$)	**1.82**	**8.63**	**43.97**	8.79	**43.76**

Table 3: **Results on CelebA dataset.** CoInD outperforms the baselines on both CS and FID across various compositionality tasks.

Tab. 3 compares CoInD against baselines in terms of CS and FID. **(1)** CoInD outperforms the baseline by $> 4\times$ in *joint*. **(2)** CoInD generates realistic faces, closer to smiling male celebrities in the held out set, as measured by FID and displayed in Fig. 5($\gamma = 1$). In App. E.3, we show that CoInD extends to Text-to-Image models by fine-tuning Stable Diffusion (Rombach et al., 2022).

CoInD provides fine-grained control over attributes. In addition to merely generating samples with conditioned attributes, CoInD can also control the *amount of attributes* in the sample. To achieve this, we introduce an attribute strength factor γ and modify the RHS of Eq. (1) as $\nabla_{\boldsymbol{X}} \log p_{\boldsymbol{\theta}}(\boldsymbol{X} \mid \text{gender}) + \gamma \nabla_{\boldsymbol{X}} \log p_{\boldsymbol{\theta}}(\boldsymbol{X} \mid \text{smiling}) - \gamma \nabla_{\boldsymbol{X}} \log p_{\boldsymbol{\theta}}(\boldsymbol{X})$. Fig. 5 shows the result of increasing γ to increase the amount of smiling in the generated image. Refer to App. E.2 for more analysis on FID and CS of CoInD.

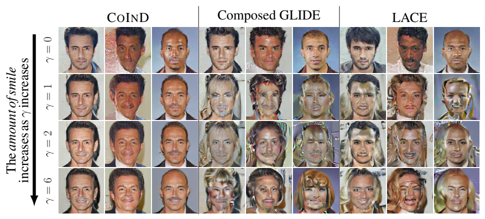

Figure 5: CoInD allows us to vary the *amount of "smile"* without affecting the gender-specific attributes. However, Composed GLIDE associates the smile attribute with the gender attribute due to their association in the training data.

6 Related Work

Our work concerns compositional generalization in generative models, where the goal is to generate data with unseen attribute compositions expressed through logical relations between attributes. One class of approaches achieves logical compositionality by combining distinct models trained for each attribute (Du et al., 2020; Liu et al., 2021; Nie et al., 2021; Du et al., 2023). In contrast, we are interested in monolithic diffusion models that learn logical compositionality. Besides being expensive and scaling linearly with the number of attributes, these models fail under practical partial support scenarios. Liu et al. (2023) studied logical compositionality broadly without differentiating between attribute supports and proposed methods to represent logical compositions in terms of *marginal* probabilities obtained through factorization of the *joint* distribution. However, these factorized sampling methods fail since the underlying generative model learns inaccurate *marginals*. In comparison, CoInD is trained to obey the independence relations from the underlying causal graph. Also, (Cho et al., 2024) note that diffusion models lack the conditional independence needed for controllability and address this with a hyperparameter during sampling. We argue that, even with disentangled features, learning accurate *marginals* tackles the root cause more effectively than such post-hoc adjustments. Encouragingly, Okawa et al. (2023) shows that compositional abilities emerge multiplicatively, and Liang et al. (2024) highlights factorization in diffusion models, suggesting they naturally exhibit compositional capabilities. However, these studies focus on generating from the *joint* distribution—a special case of logical compositionality—and are limited to binary attributes. Our work extends these ideas to more general compositions. Lastly, (Wiedemer et al., 2024) studies compositional generalization for supervised learning and provides sufficient conditions for compositionality. Our empirical observations in generative models are consistent with their theoretical results, suggesting that their findings could perhaps be extended to conditional diffusion models.

7 Conclusion

Diffusion models struggle to generate data for arbitrary attribute compositions, even when all compositions are observed during training. Existing methods represent logical relations in terms of the learned marginal distributions, assuming that the diffusion model learns the underlying conditional independence relations. We showed that this assumption does not hold in practice and worsens when only a subset of these attribute compositions are observed during training. To mitigate this problem, we proposed CoInD to train diffusion models by maximizing conditional likelihood in terms of the marginals that are obtained from the underlying causal graph using the principle of independent causal mechanisms. Our causal modeling provides CoInD a natural advantage in logical compositionality by ensuring it learns accurate marginals. Our experiments on synthetic and real image datasets highlight the theoretical benefits. CoInD shows that adequate inductive biases such as conditional independence between marginals are *necessary* for effective logical compositionality.

References

Tim Brooks, Aleksander Holynski, and Alexei A Efros. Instructpix2pix: Learning to follow image editing instructions. *arXiv preprint arXiv:2211.09800*, 2022.

Chris Burgess and Hyunjik Kim. 3d shapes dataset. https://github.com/deepmind/3dshapes-dataset/, 2018.

Wonwoong Cho, Hareesh Ravi, Midhun Harikumar, Vinh Khuc, Krishna Kumar Singh, Jingwan Lu, David I. Inouye, and Ajinkya Kale. Enhanced controllability of diffusion models via feature disentanglement and realism-enhanced sampling methods. In *European Conference on Computer Vision (ECCV)*, 2024.

Prafulla Dhariwal and Alexander Nichol. Diffusion models beat gans on image synthesis. *Advances in neural information processing systems*, 34:8780–8794, 2021.

Yilun Du and Leslie Kaelbling. Compositional generative modeling: A single model is not all you need. *arXiv preprint arXiv:2402.01103*, 2024.

Yilun Du, Shuang Li, and Igor Mordatch. Compositional visual generation with energy based models. *Advances in Neural Information Processing Systems*, 33:6637–6647, 2020.

Yilun Du, Conor Durkan, Robin Strudel, Joshua B Tenenbaum, Sander Dieleman, Rob Fergus, Jascha Sohl-Dickstein, Arnaud Doucet, and Will Sussman Grathwohl. Reduce, reuse, recycle: Compositional generation with energy-based diffusion models and mcmc. In *International conference on machine learning*, pp. 8489–8510. PMLR, 2023.

Peter J Hammond and Yeneng Sun. The essential equivalence of pairwise and mutual conditional independence. *Probability Theory and Related Fields*, 135(3):415–427, 2006.

Kaiming He, Xiangyu Zhang, Shaoqing Ren, and Jian Sun. Deep residual learning for image recognition. In *Proceedings of the IEEE conference on computer vision and pattern recognition*, pp. 770–778, 2016.

Jonathan Ho and Tim Salimans. Classifier-free diffusion guidance, 2022. URL https://arxiv.org/abs/2207.12598.

Jonathan Ho, Ajay Jain, and Pieter Abbeel. Denoising diffusion probabilistic models. *Advances in neural information processing systems*, 33:6840–6851, 2020.

Aapo Hyvärinen and Peter Dayan. Estimation of non-normalized statistical models by score matching. *Journal of Machine Learning Research*, 6(4), 2005.

Gwanghyun Kim, Taesung Kwon, and Jong Chul Ye. Diffusionclip: Text-guided diffusion models for robust image manipulation. In *Proceedings of the IEEE/CVF conference on computer vision and pattern recognition*, pp. 2426–2435, 2022.

Dohyun Kwon, Ying Fan, and Kangwook Lee. Score-based generative modeling secretly minimizes the wasserstein distance. In Alice H. Oh, Alekh Agarwal, Danielle Belgrave, and Kyunghyun Cho (eds.), *Advances in Neural Information Processing Systems*, 2022. URL https://openreview.net/forum?id=oPzICxVFqVM.

Tuomas Kynkäänniemi, Miika Aittala, Tero Karras, Samuli Laine, Timo Aila, and Jaakko Lehtinen. Applying guidance in a limited interval improves sample and distribution quality in diffusion models. *arXiv preprint arXiv:2404.07724*, 2024.

Alexander C. Li, Mihir Prabhudesai, Shivam Duggal, Ellis Brown, and Deepak Pathak. Your diffusion model is secretly a zero-shot classifier. In *Proceedings of the IEEE/CVF International Conference on Computer Vision (ICCV)*, pp. 2206–2217, October 2023.

Qiyao Liang, Ziming Liu, Mitchell Ostrow, and Ila Fiete. How diffusion models learn to factorize and compose. *arXiv preprint arXiv:2408.13256*, 2024.

Yaron Lipman, Marton Havasi, Peter Holderrieth, Neta Shaul, Matt Le, Brian Karrer, Ricky T. Q. Chen, David Lopez-Paz, Heli Ben-Hamu, and Itai Gat. Flow matching guide and code, 2024. URL https://arxiv.org/abs/2412.06264.

Nan Liu, Shuang Li, Yilun Du, Josh Tenenbaum, and Antonio Torralba. Learning to compose visual relations. *Advances in Neural Information Processing Systems*, 34:23166–23178, 2021.

Nan Liu, Shuang Li, Yilun Du, Antonio Torralba, and Joshua B. Tenenbaum. Compositional visual generation with composable diffusion models, 2023. URL https://arxiv.org/abs/2206.01714.

Ziwei Liu, Ping Luo, Xiaogang Wang, and Xiaoou Tang. Deep learning face attributes in the wild. In *International Conference on Computer Vision*, 2015.

Weili Nie, Arash Vahdat, and Anima Anandkumar. Controllable and compositional generation with latent-space energy-based models, 2021. URL https://arxiv.org/abs/2110.10873.

Maya Okawa, Ekdeep S Lubana, Robert Dick, and Hidenori Tanaka. Compositional abilities emerge multiplicatively: Exploring diffusion models on a synthetic task. In A. Oh, T. Naumann, A. Globerson, K. Saenko, M. Hardt, and S. Levine (eds.), *Advances in Neural Information Processing Systems*, volume 36, pp. 50173–50195. Curran Associates, Inc., 2023. URL https://proceedings.neurips.cc/paper_files/paper/2023/file/9d0f188c7947eacb0c07f709576824f6-Paper-Conference.pdf.

Jonas Peters, Dominik Janzing, and Bernhard Schölkopf. *Elements of causal inference: foundations and learning algorithms*. The MIT Press, 2017.

Robin Rombach, Andreas Blattmann, Dominik Lorenz, Patrick Esser, and Björn Ommer. High-resolution image synthesis with latent diffusion models. In *Proceedings of the IEEE/CVF conference on computer vision and pattern recognition*, pp. 10684–10695, 2022.

Pablo Sánchez-Moreno, Alejandro Zarzo, and Jesús S Dehesa. Jensen divergence based on fisher's information. *Journal of Physics A: Mathematical and Theoretical*, 45(12):125305, 2012.

Lukas Schott, Julius Von Kügelgen, Frederik Träuble, Peter Vincent Gehler, Chris Russell, Matthias Bethge, Bernhard Schölkopf, Francesco Locatello, and Wieland Brendel. Visual representation learning does not generalize strongly within the same domain. In *International Conference on Learning Representations*, 2020.

Maximilian Seitzer. pytorch-fid: FID Score for PyTorch. https://github.com/mseitzer/pytorch-fid, August 2020. Version 0.3.0.

Jiaming Song, Chenlin Meng, and Stefano Ermon. Denoising diffusion implicit models. *arXiv preprint arXiv:2010.02502*, 2020.

Yang Song and Stefano Ermon. Generative modeling by estimating gradients of the data distribution. *Advances in neural information processing systems*, 32, 2019.

Yang Song, Jascha Sohl-Dickstein, Diederik P Kingma, Abhishek Kumar, Stefano Ermon, and Ben Poole. Score-based generative modeling through stochastic differential equations. In *International Conference on Learning Representations*, 2021. URL https://openreview.net/forum?id=PxTIG12RRHS.

Amos Storkey. When training and test sets are different: Characterizing learning transfer. In *Dataset Shift in Machine Learning*. The MIT Press, 2008.

Max Welling and Yee W Teh. Bayesian learning via stochastic gradient langevin dynamics. In *Proceedings of the 28th international conference on machine learning (ICML-11)*, pp. 681–688. Citeseer, 2011.

Thaddäus Wiedemer, Prasanna Mayilvahanan, Matthias Bethge, and Wieland Brendel. Compositional generalization from first principles. *Advances in Neural Information Processing Systems*, 36, 2024.

Appendix

Table of Contents

A Preliminaries of Score-based Models

Score-based models Score-based models (Song et al., 2021) learn the score of the observed data distribution, $P_{\text{train}}(\boldsymbol{X})$ through score matching (Hyvärinen & Dayan, 2005). The score function $s_{\boldsymbol{\theta}}(\mathbf{x}) = \nabla_{\mathbf{x}} \log p_{\boldsymbol{\theta}}(\mathbf{x})$ is learned by a neural network parameterized by $\boldsymbol{\theta}$.

$$L_{\text{score}} = \mathbb{E}_{\mathbf{x}\sim p_{\text{train}}}\left[\|s_{\boldsymbol{\theta}}(\mathbf{x}) - \nabla_{\mathbf{x}} \log p_{\text{train}}(\mathbf{x})\|_2^2\right] \tag{8}$$

During inference, sampling is performed using Langevin dynamics:

$$\mathbf{x}_t = \mathbf{x}_{t-1} + \frac{\eta}{2}\nabla_{\mathbf{x}} \log p_{\boldsymbol{\theta}}(\mathbf{x}_{t-1}) + \sqrt{\eta}\epsilon_t, \quad \epsilon_t \sim \mathcal{N}(0,1) \tag{9}$$

where $\eta > 0$ is the step size. As $\eta \to 0$ and $T \to \infty$, the samples $\mathbf{x}_t$ converge to $p_{\boldsymbol{\theta}}(\boldsymbol{X})$ under certain regularity conditions (Welling & Teh, 2011).

Diffusion models Song & Ermon (2019) proposed a scalable variant that involves adding noise to the data Ho et al. (2020) has shown its equivalence to Diffusion models. Diffusion models are trained by adding noise to the image $\mathbf{x}$ according to a noise schedule, and then neural network, ϵ_θ is used to predict the noise from the noisy image, $\mathbf{x_t}$. The training objective of the diffusion models is given by:

$$L_{\text{score}} = \mathbb{E}_{\mathbf{x}\sim p_{\text{train}}}\mathbb{E}_{t\sim[0,T]}\left\|\epsilon - \epsilon_\theta\left(\mathbf{x}_t, t\right)\right\|^2 \tag{10}$$

Here, the perturbed data $\mathbf{x}_t$ is expressed as: $\mathbf{x}_t = \sqrt{\bar{\alpha}_t}\mathbf{x} + \sqrt{1-\bar{\alpha}_t}\epsilon$ where $\bar{\alpha}_t = \prod_{i=1}^{T}\alpha_i$, for a pre-specified noise schedule α_t. The score can be obtained using,

$$s_\theta(\mathbf{x}_t, t) \approx -\frac{\epsilon_\theta(\mathbf{x}_t, t)}{\sqrt{1-\bar{\alpha}_t}} \tag{11}$$

Langevin dynamics can be used to sample from the $s_\theta(\mathbf{x}_t, t)$ to generate samples from $p(\boldsymbol{X})$. The conditional score (Dhariwal & Nichol, 2021) is used to obtain samples from the conditional distribution $p_{\boldsymbol{\theta}}(\boldsymbol{X} \mid C)$ as:

$$\nabla_{\boldsymbol{X}_t} \log p(\boldsymbol{X}_t \mid C) = \underbrace{\nabla_{\boldsymbol{X}_t} \log p_{\boldsymbol{\theta}}(\boldsymbol{X}_t)}_{\text{Unconditional score}} + \gamma\nabla_{\boldsymbol{X}_t} \log \underbrace{p_{\boldsymbol{\theta}}(C \mid \boldsymbol{X}_t)}_{\text{noisy classifier}}$$

where γ is the classifier strength. Instead of training a separate noisy classifier, Ho & Salimans have extended to conditional generation by training $\nabla_{\boldsymbol{X}_t} \log p_{\boldsymbol{\theta}}(\boldsymbol{X}_t \mid C) = s_\theta(\boldsymbol{X}_t, t, C)$. The sampling can be performed using the following equation:

$$\nabla_{\boldsymbol{X}_t} \log p(\boldsymbol{X}_t \mid C) = (1-\gamma)\nabla_{\boldsymbol{X}_t} \log p_{\boldsymbol{\theta}}(\boldsymbol{X}_t) + \gamma\nabla_{\boldsymbol{X}_t} \log p_{\boldsymbol{\theta}}(\boldsymbol{X}_t \mid C) \tag{12}$$

However, the sampling needs access to unconditional scores as well. Instead of modelling $\nabla_{\boldsymbol{X}_t} \log p_{\boldsymbol{\theta}}(\boldsymbol{X}_t)$, $\nabla_{\boldsymbol{X}_t} \log p_{\boldsymbol{\theta}}(\boldsymbol{X}_t|C)$ as two different models Ho & Salimans have amortize training a separate classifier training a conditional model $s_\theta(\mathbf{x}_t, t, \mathbf{c})$ jointly with unconditional model trained by setting $c = \varnothing$.

In the general case of classifier-free guidance, a single model can be effectively trained to accommodate all subsets of attribute distributions. During the training phase, each attribute c_i is randomly set to $\varnothing$ with a probability p_{uncond}. This approach ensures that the model learns to match all possible subsets of attribute distributions. Essentially, through this formulation, we use the same network to model all the possible subsets of conditional probability.

Once trained, the model can generate samples conditioned on specific attributes, such as c_i and c_j, by setting all other conditions to $\varnothing$. The conditional score is then computed as, $\nabla_{\boldsymbol{X}_t} \log p_{\boldsymbol{\theta}}(\boldsymbol{X}_t|c_i, c_j) = \mathbf{x}_t, \mathbf{c}^{i,j})$, where $\mathbf{c}^{i,j}$ represents the condition vector with all values other than i and j set to $\varnothing$. This method allows for flexible and efficient sampling across various attribute combinations.

Estimating Guidance Once the diffusion model is trained, we investigate the implicit classifier, $p_\theta(C|\boldsymbol{X})$, learned by the model. This will give us insights into the learning process of the diffusion models. (Li et al., 2023) have shown a way to calculate $p_\theta(C_i = c_i \mid \boldsymbol{X} = \mathbf{x})$, borrowing equation (5), (6) from (Li et al., 2023).

$$p_\theta(C_i = c_i \mid \mathbf{x}) = \frac{p(c_i)\, p_\theta(\mathbf{x} \mid c_i)}{\sum_k p(c_k)\, p_\theta(\mathbf{x} \mid c_k)}$$

$$p_\theta(C_i = c_i \mid \mathbf{x}) = \frac{\exp\{-\mathbb{E}_{t,\epsilon}[\|\epsilon - \epsilon_\theta(\mathbf{x}_t, t, \mathbf{c}^i)\|^2]\}}{\mathbb{E}_{C_i}\left[\exp\{-\mathbb{E}_{t,\epsilon}[\|\epsilon - \epsilon_\theta(\mathbf{x}_t, t, \mathbf{c}^i)\|^2]\}\right]} \tag{13}$$

Likewise, we can extend it to joint distribution by

$$p_\theta(C_i = c_i, C_j = c_j \mid \mathbf{x}) = \frac{\exp\{-\mathbb{E}_{t,\epsilon}[\|\epsilon - \epsilon_\theta(\mathbf{x}_t, t, \mathbf{c}^{i,j})\|^2]\}}{\mathbb{E}_{C_i, C_j}\left[\exp\{-\mathbb{E}_{t,\epsilon}[\|\epsilon - \epsilon_\theta(\mathbf{x}_t, t, \mathbf{c}^{i,j})\|^2]\}\right]} \tag{14}$$

Practical Implementation The authors Li et al.. have showed many axproximations to compute $\mathbb{E}_{t,\epsilon}$. However, we use a different approximation inspired by Kynkäänniemi et al. (2024), where we sample 5 time-steps between [300,600] instead of these time-steps spread over the [0, T].

B Proofs for Claims

In this section, we detail the mathematical derivations for case study from § 3 in App. B.1, relate the origin of the conditional independence violation to the loss function of vanilla diffusion models in App. B.2, and then derive the final loss function of CoInD in App. B.3.

B.1 Proof for the case study in § 3

In this section, we prove that failure of compositionality in diffusion models is due to the violation of conditional independence.

The causal graph shown in Fig. 2a provides us with the following conditional independence relation:

$$p(C \mid X) = \prod_i p(C_i \mid X) \tag{CI relation}$$

This CI relation is used by several works (Liu et al., 2023; Nie et al., 2021), including ours, to derive the expression for the joint distribution $p(X \mid C)$ in terms of the marginals $p(X \mid C_i)$ for logical compositionality. As a reminder, logical compositionality is preferred over simple conditional generation as it (1) provides fine-grained control over the attributes, (2) facilitates NOT relations on attributes, and (3) is more interpretable. The joint likelihood is written in terms of the marginals using the CI relation and the causal factorization as,

$$p(X \mid C) = \frac{p(X)}{p(C)} \prod_i \left(\frac{p(X \mid C_i) p(C_i)}{p(X)} \right) \tag{JM relation}$$

JM relation is obtained by applying bayes' on all terms of CI. Note that CI relation is crucial for JM relation to hold. Applying $\nabla_{\boldsymbol{X}}(\cdot)$ to the equation will result in the score form of JM relation which we call is SJM equation, given as:

$$\nabla_{\boldsymbol{X}} \log p_\theta(X \mid C) = \nabla_{\mathbf{X}} \log p_\theta(\mathbf{X}) + \sum_i \left[\nabla_{\mathbf{X}} \log p_\theta(\mathbf{X} \mid C_i) - \nabla_{\mathbf{X}} \log p_\theta(\mathbf{X})\right] \tag{ SJM relation}$$

Sample from joint likelihood using the score of LHS of SJM relation, referred to as joint sampling in § 3. Similarly, we sample using the score of RHS of SJM relation, referred to as marginal sampling in § 3. If the learned generative model satisfies the JM relation, then there should not be any difference in the CS between joint sampling and marginal sampling. However, in Tab. 1, we see a drop in CS, implying JM relation is not satisfied in the learned model.

JM relation must hold in the learned generative model if CI relation is true in the learned generative model. Therefore, we check if the CI relation holds in the generative model by measuring JSD between LHS and RHS of CI relation as shown in Eq. (32). The results Tab. 1 confirm that the CI relation does not hold in the learned model. This is a significant finding since existing works (Liu et al., 2023; Nie et al., 2021) blindly trust the model to satisfy CI relation, leading to severe performance drop when the training support is non-uniform or partial.

The CI relation is violated in the learned model because the standard training objective is not suitable for compositionality, as it does not account for the incorrect $p_{\text{train}}(X \mid C_i)$. The proof is detailed in the next section App. B.2. Therefore, we proposed CoInD to ensure the JM relation was satisfied by explicitly learning the marginal likelihood according to the causal factorization.

B.2 Standard diffusion model objective is not suitable for logical compositionality

This section proves that the violation in conditional independence in diffusion models is due to learning incorrect marginals, $p_{\text{train}}(\boldsymbol{X} \mid C_i)$ under $C_i \not\perp\!\!\!\perp C_j$. We leverage the causal invariance property: $p_{\text{train}}(\boldsymbol{X} \mid C) = p_{\text{true}}(\boldsymbol{X} \mid C)$, where p_{train} is the training distribution and p_{true} is the true underlying distribution.

Consider the training objective of the score-based models in classifier free formulation Eq. (8). For the classifier-free guidance, a single model $s_{\boldsymbol{\theta}}(\mathbf{x}, C)$ is effectively trained to match the score of all subsets of attribute distributions. Therefore, the effective formulation for classifier-free guidance can be written as,

$$L_{\text{score}} = \mathbb{E}_{\mathbf{x}\sim p_{\text{train}}}\mathbb{E}_S\left[\|\nabla_{\mathbf{x}} \log p_{\boldsymbol{\theta}}(\mathbf{x} \mid c_S) - \nabla_{\mathbf{x}} \log p_{\text{train}}(\mathbf{x} \mid c_S)\|_2^2\right] \tag{15}$$

where S is the power set of attributes.

From the properties of Fisher divergence, $L_{\text{score}} = 0$ iff $p_{\boldsymbol{\theta}}(\boldsymbol{X} \mid c_S) = p_{\text{train}}(\boldsymbol{X} \mid c_S)$, $\forall S$. In the case of marginals, $p_{\boldsymbol{\theta}}(\boldsymbol{X} \mid C_i)$ i.e. $S = \{C_i\}$ for some $1 \leq i \leq n$,

$$\begin{aligned}
p_{\boldsymbol{\theta}}(\boldsymbol{X} \mid C_i) &= p_{\text{train}}(\boldsymbol{X} \mid C_i) \\
&= \sum_{C_{-i}} p_{\text{train}}(\boldsymbol{X} \mid C_i, C_{-i}) p_{\text{train}}(C_{-i} \mid C_i) \\
&= \sum_{C_{-i}} p_{\text{true}}(\boldsymbol{X} \mid C_i, C_{-i}) p_{\text{train}}(C_{-i} \mid C_i) \\
&\neq \sum_{C_{-i}} p_{\text{true}}(\boldsymbol{X} \mid C_i, C_{-i}) p_{\text{true}}(C_{-i}) = p_{\text{true}}(\boldsymbol{X} \mid C_i) \\
\implies p_{\boldsymbol{\theta}}(\boldsymbol{X} \mid C_i) &\neq p_{\text{true}}(\boldsymbol{X} \mid C_i)
\end{aligned} \tag{16}$$

Where $C_{-i} = \prod_{\substack{j=1 \\ j\neq i}}^{n} C_j$, which is every attribute except C_i. Therefore, the objective of the score-based models is to maximize the likelihood of the marginals of training data and not the true marginal distribution, which is different from the training distribution when $C_i \not\perp\!\!\!\perp C_j$.

B.3 Step-by-step derivation of CoInD in § 4

The objective is to train the model by explicitly modeling the joint likelihood following the causal factorization from Eq. (JM relation). The minimization for this objective can be written as,

$$\mathcal{L}_{\text{comp}} = \mathcal{W}_2\left(p(\boldsymbol{X} \mid C), \frac{p_{\boldsymbol{\theta}}(\boldsymbol{X})}{p_{\boldsymbol{\theta}}(C)} \prod_i \frac{p_{\boldsymbol{\theta}}(\boldsymbol{X} \mid C_i) p_{\boldsymbol{\theta}}(C_i)}{p_{\boldsymbol{\theta}}(\boldsymbol{X})}\right) \tag{17}$$

where $\mathcal{W}_2$ is 2-Wasserstein distance. Applying the triangle inequality to Eq. (17) we have,

$$\mathcal{L}_{\text{comp}} \leq \underbrace{\mathcal{W}_2\left(p(\boldsymbol{X} \mid C), p_{\boldsymbol{\theta}}(\boldsymbol{X} \mid C)\right)}_{\text{Distribution matching}} + \underbrace{\mathcal{W}_2\left(p_{\boldsymbol{\theta}}(\boldsymbol{X} \mid C), \frac{p_{\boldsymbol{\theta}}(\boldsymbol{X})}{p_{\boldsymbol{\theta}}(C)} \prod_i^n \frac{p_{\boldsymbol{\theta}}(\boldsymbol{X} \mid C_i) p_{\boldsymbol{\theta}}(C_i)}{p_{\boldsymbol{\theta}}(\boldsymbol{X})}\right)}_{\text{Conditional Independence}} \tag{18}$$

(Kwon et al., 2022) showed that under some conditions, the Wasserstein distance between $p_0(\boldsymbol{X}), q_0(\boldsymbol{X})$ is upper bounded by the square root of the score-matching objective. Rewriting Equation 16 from (Kwon et al., 2022)

$$\mathcal{W}_2\left(p_0(\boldsymbol{X}), q_0(\boldsymbol{X})\right) \leq K\sqrt{\mathbb{E}_{p_0(\boldsymbol{X})}\left[||\nabla_{\boldsymbol{X}} \log p_0(\boldsymbol{X}) - \nabla_{\boldsymbol{X}} \log q_0(\boldsymbol{X})||_2^2\right]} \tag{19}$$

Distribution matching Following Eq. (19) result, the first term in Eq. (18), replacing p_0 as p and q_0 as p_θ will result in

$$\begin{aligned}
\mathcal{W}_2\left(p(\boldsymbol{X} \mid C), p_{\boldsymbol{\theta}}(\boldsymbol{X} \mid C)\right) &\leq K_1\sqrt{\mathbb{E}_{p_0(\boldsymbol{X})}\left[||\nabla_{\boldsymbol{X}} \log p(\boldsymbol{X} \mid C) - \nabla_{\boldsymbol{X}} \log p_\theta(\boldsymbol{X})||_2^2\right]} \\
&= K_1\sqrt{\mathcal{L}_{\text{score}}}
\end{aligned} \tag{20}$$

Conditional Independence Following Eq. (19) result, the second term in Eq. (18), replacing p_0 as p_θ and $q_0(\boldsymbol{X})$ as $\frac{p_{\boldsymbol{\theta}}(\boldsymbol{X})}{p_{\boldsymbol{\theta}}(C)} \prod_i^n \frac{p_{\boldsymbol{\theta}}(\boldsymbol{X}|C_i)p_{\boldsymbol{\theta}}(C_i)}{p_{\boldsymbol{\theta}}(\boldsymbol{X})}$

$$\mathcal{W}_2\left(p_{\boldsymbol{\theta}}(\boldsymbol{X} \mid C), \frac{p_{\boldsymbol{\theta}}(\boldsymbol{X})}{p_{\boldsymbol{\theta}}(C)} \prod_i^n \frac{p_{\boldsymbol{\theta}}(\boldsymbol{X} \mid C_i)p_{\boldsymbol{\theta}}(C_i)}{p_{\boldsymbol{\theta}}(\boldsymbol{X})}\right)$$
$$\leq \sqrt{\mathbb{E}\|\nabla_{\mathbf{X}} \log p_\theta(\boldsymbol{X} \mid C) - \nabla_{\mathbf{X}} \log \frac{p_{\boldsymbol{\theta}}(\boldsymbol{X})}{p_{\boldsymbol{\theta}}(C)} \prod_i^n \frac{p_{\boldsymbol{\theta}}(\boldsymbol{X} \mid C_i)p_{\boldsymbol{\theta}}(C_i)}{p_{\boldsymbol{\theta}}(\boldsymbol{X})}\|_2^2}$$

Further simplifying and incorporating $\nabla_{\mathbf{X}} \log p_\theta(C_i) = 0$ and $\nabla_{\mathbf{X}} \log p_\theta(C) = 0$ will result in

$$\mathcal{W}_2\left(p_{\boldsymbol{\theta}}(\boldsymbol{X} \mid C), \frac{p_{\boldsymbol{\theta}}(\boldsymbol{X})}{p_{\boldsymbol{\theta}}(C)} \prod_i^n \frac{p_{\boldsymbol{\theta}}(\boldsymbol{X} \mid C_i)p_{\boldsymbol{\theta}}(C_i)}{p_{\boldsymbol{\theta}}(\boldsymbol{X})}\right)$$
$$\leq K_2 \sqrt{\underbrace{\mathbb{E}\|\nabla_{\mathbf{X}} \log p_\theta(\boldsymbol{X} \mid C) - \nabla_{\mathbf{X}} \log p_\theta(\boldsymbol{X}) - \sum_i \left[\nabla_{\mathbf{X}} \log p_\theta(\boldsymbol{X} \mid C_i) - \nabla_{\mathbf{X}} \log p_\theta(\boldsymbol{X})\right] \|_2^2}_{\mathcal{L}_{\text{CI}}}}$$
$$= K_2 \sqrt{\mathcal{L}_{\text{CI}}} \tag{21}$$

Substituting Eq. (20), Eq. (21) in Eq. (18) will result in our final learning objective

$$\mathcal{L}_{\text{comp}} \leq K_1 \sqrt{\mathcal{L}_{\text{score}}} + K_2 \sqrt{\mathcal{L}_{\text{CI}}} \tag{22}$$

where K_1, K_2 are positive constants, i.e., the conditional independence objective $\mathcal{L}_{\text{CI}}$ is incorporated alongside the existing score-matching loss $\mathcal{L}_{\text{score}}$.

Note that Eq. (21) is the Fisher divergence between the joint $p_\theta(\boldsymbol{X} \mid C)$ and the causal factorization $\frac{p_\theta(X)}{p_\theta(C)} \prod_i \frac{p_\theta(\boldsymbol{X}|C_i)p_\theta(C_i)}{p_\theta(\boldsymbol{X})}$ from Eq. (JM relation). From the properties of Fisher divergence (Sánchez-Moreno et al., 2012), $\mathcal{L}_{\text{CI}} = 0$ iff $p_\theta(\boldsymbol{X} \mid C) = \frac{p_\theta(\boldsymbol{X})}{p_\theta(C)} \prod_i^n \frac{p_\theta(\boldsymbol{X}|C_i)p_\theta(C_i)}{p_\theta(\boldsymbol{X})}$ and further implying, $\prod_i p_\theta(C_i \mid \boldsymbol{X}) = p_{\text{train}}(C \mid \boldsymbol{X})$

When $L_{\text{comp}} = 0$: $P_\theta(\boldsymbol{X} \mid C) = P_{\text{train}}(\boldsymbol{X} \mid C) = P(\boldsymbol{X} \mid C)$, and $\prod_i p_\theta(C_i \mid \boldsymbol{X}) = p_{\text{train}}(C \mid \boldsymbol{X})$. This implies that the learned marginals obey the causal independence relations from the data-generation process, leading to more accurate marginals.

C Practical Considerations

To facilitate scalability and numerical stability for optimization, we introduce two approximations to the upper bound of our objective function Eq. (4).

C.1 Scalability of $\mathcal{L}_{\text{CI}}$

A key computational challenge posed by Eq. (6) is that the number of model evaluations grows linearly with the number of attributes. The Eq. (6) is derived from conditional independence formulation as follows:

$$p_\theta(C \mid X) = \prod_i p_\theta(C_i \mid X). \tag{23}$$

By applying Bayes' theorem to all terms, we obtain,

$$\frac{p_\theta(\boldsymbol{X} \mid C)p_\theta(C)}{p_\theta(X)} = \prod_i \frac{p_\theta(\boldsymbol{X} \mid C_i)p_\theta(C_i)}{p_\theta(\boldsymbol{X})} \tag{24}$$

Note that this formulation is equal to the causal factorization. From this, by applying logarithm and differentiating w.r.t. $\boldsymbol{X}$, we derive the score formulation.

$$\nabla_{\boldsymbol{X}} \log p_\theta(\boldsymbol{X} \mid C) = \nabla_{\boldsymbol{X}} \log \sum_i p_\theta(\boldsymbol{X} \mid C_i) - \nabla_{\boldsymbol{X}} \log p_\theta(\boldsymbol{X}) \tag{25}$$

The L_2 norm of the difference between LHS and RHS of the objective in Eq. (25) is given by, which forms our $\mathcal{L}_{\text{CI}}$ objective.

$$\mathcal{L}_{\text{CI}} = \|\nabla_{\boldsymbol{X}} \log p_\theta(\boldsymbol{X} \mid C) - \left(\nabla_{\boldsymbol{X}} \log \sum_i p_\theta(\boldsymbol{X} \mid C_i) - \nabla_{\boldsymbol{X}} \log p_\theta(\boldsymbol{X})\right)\|_2^2 \tag{26}$$

Due to the $\sum_i$, in the equation, the number of model evaluations grows linearly with the number of attributes (n). This $\mathcal{O}(n)$ computational complexity hinders the approach's applicability at scale. To address this, we leverage the results of (Hammond & Sun, 2006), which shows conditional independence is equivalent to pairwise independence under large n to reduce the complexity to $\mathcal{O}(1)$ in expectation. This allows for a significant improvement in scalability while maintaining computational efficiency. Using this result, we modify Eq. (23) to:

$$p_\theta(C_i, C_j \mid X) = p_\theta(C_i \mid X) p_\theta(C_j \mid X). \quad \forall i, j$$

Accordingly, we can simplify the loss function for conditional independence as follows:

$$\mathcal{L}_{\text{CI}} = \mathbb{E}_{p(\boldsymbol{X},C)} \mathbb{E}_{j,k} \|\nabla_X [\log p_\theta(X|C_j, C_k) - \log p_\theta(X|C_j) - \log p_\theta(X|C_k) + \log p_\theta(X)]\|_2^2. \tag{27}$$

In score-based models, which are typically neural networks, the final objective is given as:

$$\mathcal{L}_{\text{CI}} = \mathbb{E}_{p(\boldsymbol{X},C)} \mathbb{E}_{j,k} \|s_{\boldsymbol{\theta}}(\boldsymbol{X}, C_j, C_k) - s_{\boldsymbol{\theta}}(\boldsymbol{X}, C_j) - s_{\boldsymbol{\theta}}(\boldsymbol{X}, C_k) + s_{\boldsymbol{\theta}}(\boldsymbol{X}, \varnothing)\|_2^2 \tag{28}$$

where $s_{\boldsymbol{\theta}}(\cdot) \coloneqq \nabla_{\boldsymbol{X}} \log p_\theta(\cdot)$ is the score of the distribution modeled by the neural network. We leverage classifier-free guidance to train the conditional score $s_{\boldsymbol{\theta}}(\boldsymbol{X}, C_i)$ by setting $C_k = \varnothing$ for all $k \neq i$, and likewise for $s_{\boldsymbol{\theta}}(\boldsymbol{X}, C_i, C_j)$, we set $C_k = \varnothing$ for all $k \notin \{i, j\}$.

C.2 Simplification of Theoretical Loss

In Eq. (4), we showed that the 2-Wassertein distance between the true joint distribution $p(\boldsymbol{X} \mid C)$ and the causal factorization in terms of the marginals $p(\boldsymbol{X} \mid C_i)$ is upper bounded by the weighted sum of the square roots of $\mathcal{L}_{\text{score}}$ and $\mathcal{L}_{\text{CI}}$ as $\mathcal{L}_{\text{comp}} \leq K_1 \sqrt{\mathcal{L}_{\text{score}}} + K_2 \sqrt{\mathcal{L}_{\text{CI}}}$. In practice, however, we minimized a simple weighted sum of $\mathcal{L}_{\text{score}}$ and $\mathcal{L}_{\text{CI}}$, given by $\mathcal{L}_{\text{final}} = \mathcal{L}_{\text{score}} + \lambda \mathcal{L}_{\text{CI}}$ as shown in Eq. (7) instead of Eq. (4). We used Eq. (7) to avoid the instability caused by larger gradient magnitudes (due to the square root). Eq. (7) also provided the following practical advantages: **(1)** the simplicity of the loss function that made hyperparameter tuning easier, and **(2)** the similarity of Eq. (7) to the loss functions of pre-trained diffusion models allowing us to reuse existing hyperparameter settings from these models. We did not observe any significant difference in conclusion between the models trained on Eq. (4) and Eq. (7) as shown in Tabs. 4 and 5. Both approaches significantly outperformed the baselines.

Support	Method	JSD ↓	$\wedge$ (CS) ↑	$\neg$ Color (CS)↑	$\neg$ Digit (CS) ↑
Uniform	LACE	-	96.40	92.56	83.67
	Composed GLIDE	0.16	98.15	99.30	81.64
	Theoretical CoInD Eq. (4)	0.12	98.44	**100.00**	81.25
	CoInD ($\lambda = 0.2$)	0.14	99.73	99.32	84.94
	CoInD ($\lambda = 1.0$)	**0.10**	**99.99**	99.33	**89.60**
Non-uniform	LACE	-	82.61	65.16	69.51
	Composed GLIDE	0.30	86.10	81.61	70.44
	Theoretical CoInD Eq. (4)	0.17	96.88	**93.75**	72.66
	CoInD ($\lambda = 1.0$)	**0.15**	**99.95**	92.41	**84.98**
Partial	LACE	-	10.85	9.03	28.24
	Composed GLIDE	2.75	7.40	5.09	33.86
	Theoretical CoInD Eq. (4)	**1.11**	23.44	**64.84**	**53.12**
	CoInD ($\lambda = 1.0$)	1.17	**52.38**	53.28	52.59

Table 4: Results on Colored MNIST to directly minimize the upper bound ($K_1 = 1, K_2 = 0.1$)

Support	Method	JSD ↓	∧ Composition		¬ Composition	
			R^2 ↑	CS ↑	R^2↑	CS↑
Uniform	LACE	-	0.97	91.19	0.85	50.00
	Composed GLIDE	0.302	0.94	83.75	0.91	48.43
	Theoretical CoInD Eq. (4)	0.270	0.98	92.19	0.92	**64.06**
	CoInD ($\lambda = 1.0$)	**0.215**	0.98	**95.31**	0.92	55.46
Partial	LACE	-	0.88	62.07	0.70	30.10
	Composed GLIDE	0.503	0.86	51.56	0.61	34.63
	Theoretical CoInD Eq. (4)	0.450	0.93	78.13	0.88	51.56
	CoInD ($\lambda = 1.0$)	**0.287**	**0.97**	**91.10**	**0.92**	**53.90**

Table 5: Results on Shapes3D with the objective of directly minimizing the upper bound Eq. (4) ($K_1 = 1$, $K_2 = 0.1$)

C.3 Choice of Hyperparameter λ

Effect of λ on the Learned Conditional Independence.

CoInD enforces conditional independence between the marginals of the attributes learned by the model by minimizing $\mathcal{L}_{\text{CI}}$ defined in Eq. (28). Here, we investigate the effect of $\mathcal{L}_{\text{CI}}$ on the effectiveness of logical compositionality by varying its strength through λ in Eq. (7). Figure 6 plots JSD and CS ($\wedge$) as functions of λ for models trained on the Colored MNIST dataset under the diagonal partial support setting. When $\lambda = 0$, training relies solely on the score matching loss, resulting in higher conditional dependence between $C_i \mid \boldsymbol{X}$. As λ increases, CS improves since ensuring conditional independence between the marginals also encourages more accurate learning of the true marginals. However, when λ takes large values, the model learns truly independent conditional distribution $C \mid \boldsymbol{X}$ but effectively ignores the input compositions and generates samples based solely on the prior distribution $p_{\boldsymbol{\theta}}(\boldsymbol{X})$. As a result, CS drops.

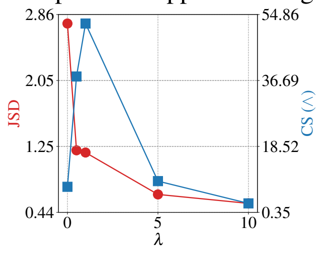

Figure 6: Effect of λ on logical compositionality under diagonal partial support on the Colored MNIST dataset.

The value for the hyperparameter λ is chosen such that the gradients from the score-matching objective L_{score} and the conditional independence objective L_{CI} are balanced in magnitude. One way to choose λ is by training a vanilla diffusion model and setting $\lambda = \frac{L_{score}}{L_{CI}}$. As a rule of thumb, we recommend the simplified setting: $\lambda = L_{score} \times 4000$. We used two values for λ in our experiments and noticed that they gave similar results, indicating that the approach was stable for various values of λ.

D Experiment Details

D.1 CoInD Algorithm

To compute pairwise independence in a scalable fashion, we randomly select two attributes, i and j, for a sample in the batch and enforce independence between them. As the score in Eq. (11) is given by $\frac{\epsilon_\theta(\mathbf{x}_t,t)}{\sqrt{1-\bar{\alpha}_t}}$. The final equation for enforcing $\mathcal{L}_{\text{CI}}$ will be:

$$L_{CI} = \frac{1}{1-\bar{\alpha}_t}\left\|\boldsymbol{\epsilon}_\theta(\mathbf{x}_t,t,\mathbf{c}^i) + \boldsymbol{\epsilon}_\theta(\mathbf{x}_t,t,\mathbf{c}^j) - \boldsymbol{\epsilon}_\theta(\mathbf{x}_t,t,\mathbf{c}^{i,j}) - \boldsymbol{\epsilon}_\theta(\mathbf{x}_t,t,\mathbf{c}^{\varnothing})\right\|_2^2$$

We follow Ho et al. (2020) to weight the term by $1 - \bar{\alpha}_t$. This results in an algorithm for CoInD, requiring only a few modifications of lines from (Ho & Salimans, 2022), highlighted below. **Practical Implementation** In our experiments, we have used $p_{\text{uncond}} = 0.3$ and for Shapes3D instead of enforcing $C_i \perp\!\!\!\perp C_j \mid X$, for all i, j enforcing $C_i \perp\!\!\!\perp C_{-i} \mid X$ for all i have led to slightly better results.

Algorithm 1 CoInD Training

```
1: repeat
2:   $(\mathbf{c}, \mathbf{x}_0) \sim p_{\text{train}}(\mathbf{c}, x)$
3:   $c_k \leftarrow \varnothing$ with probability $p_{uncond}$        ▷ Set element of index,$k$ i.e, $c_k$ to $\varnothing$ with $p_{uncond} \forall k \in [0, N]$
   probability
4:   $i \sim \text{Uniform}(\{0, \dots, N\}), j \sim \text{Uniform}(\{0, \dots, N\} \setminus \{i\})$        ▷ Select two random attribute indices
5:   $t \sim \text{Uniform}(\{1, \dots, T\})$
6:   $\boldsymbol{\epsilon} \sim \mathcal{N}(\mathbf{0}, \mathbf{I})$
7:   $x_t = \sqrt{\bar{\alpha}_t}\mathbf{x}_0 + \sqrt{1 - \bar{\alpha}_t}\boldsymbol{\epsilon}$
8:   $\mathbf{c}^i, \mathbf{c}^j, \mathbf{c}^{i,j} \leftarrow \mathbf{c}$
9:   $\mathbf{c}^i \leftarrow \{c_k = \varnothing \mid k \neq i\}, \mathbf{c}^j \leftarrow \{c_k = \varnothing \mid k \neq j\}, \mathbf{c}^{i,j} \leftarrow \{c_k = \varnothing \mid k \notin \{i, j\}\}, \mathbf{c}^{\varnothing} \leftarrow \varnothing$
10:  $L_{CI} = ||\boldsymbol{\epsilon}_\theta(\mathbf{x}_t, t, \mathbf{c}^i) + \boldsymbol{\epsilon}_\theta(\mathbf{x}_t, t, \mathbf{c}^j) - \boldsymbol{\epsilon}_\theta(\mathbf{x}_t, t, \mathbf{c}^{i,j}) - \boldsymbol{\epsilon}_\theta(\mathbf{x}_t, t, \mathbf{c}^{\varnothing})||_2^2$
11:  Take gradient descent step one
       $\nabla_\theta[\|\boldsymbol{\epsilon} - \boldsymbol{\epsilon}_\theta(\mathbf{x}_t, t, \mathbf{c})\|^2 + \lambda L_{CI}]$
12: until converged
```

D.2 Details of Logical Compositionality Task

We designed the following task to evaluate two primitive logical compositions. **(1)** AND Composition $\wedge$, **(2)** NOT Composition $\neg$

AND Composition To evaluate the $\wedge$ composition, we apply the $\wedge$ operation over all the attributes to generate a respective image. Consider an image from the Shapes3D dataset (see Figure Fig. 7). The image is generated by some function, f, with the input $c = [\; 6 \;\; 8 \;\; 4 \;\; 6 \;\; 2 \;\; 11 \;]$. The following image can be queried using the logical expression $C_1 = 6 \wedge \dots \wedge C_6 = 11$. We follow Equation Eq. (1) to sample from the above logical composition. To reiterate, for the $\wedge$ composition task on Shapes3D, the sampling equation is given by $\nabla_{\boldsymbol{X}} p_{\boldsymbol{\theta}}(\boldsymbol{X} \mid C_1 = 6 \wedge \dots \wedge C_6 = 11)$:

$$\nabla_{\mathbf{X}} \log p_{\boldsymbol{\theta}}(\boldsymbol{X}) + \sum_i [\nabla_{\mathbf{X}} \log p_{\boldsymbol{\theta}}(\boldsymbol{X} \mid C_i) - \nabla_{\mathbf{X}} \log p_{\boldsymbol{\theta}}(\boldsymbol{X})] \tag{29}$$

Similarly, to evaluate the AND composition for the Colored MNIST dataset, we perform the $\wedge$ operation over digit C_1 and color C_2.

NOT Composition To evaluate the $\neg$ compositions, the image is queried as an AND on all the attributes except the object attribute, which is queried by its negation. For example, consider the same image from Figure Fig. 7, where the object sphere ($C_5 = 2$) can be expressed as $C_5 = \neg[0 \vee 1 \vee 3]$, because the object class can only take four possible values. Therefore, the same image can be described as $C_1 = 6 \wedge \dots \wedge C_5 = \neg[0 \vee 1 \vee 3] \dots \wedge C_6 = 11$. The only possible generation that meets these criteria is the image displayed as expected.

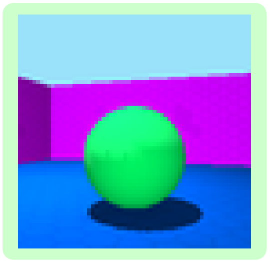
Figure 7: Image from Shapes3d with attributes $c = [6, 8, 4, 6, 2, 11]$

The sampling equation for a test image with attributes $C_1, C_2, C_3, C_4, C_5, C_6$ can be written as $C_1 = 6 \wedge C_2 = 8 \wedge C_3 = 4 \wedge C_4 = 6 \wedge C_5 = \neg[0 \vee 1 \vee 3] \wedge C_6 = 11$. Following Eq. (2), the sampling equation is written as follows:

$$\begin{aligned}&\nabla_{\mathbf{X}} \log p_{\boldsymbol{\theta}}(\boldsymbol{X}|C_1 = 6) + \nabla_{\mathbf{X}} \log p_{\boldsymbol{\theta}}(\boldsymbol{X}|C_2 = 8) + \nabla_{\mathbf{X}} \log p_{\boldsymbol{\theta}}(\boldsymbol{X}|C_3 = 4)\\ &+\nabla_{\mathbf{X}} \log p_{\boldsymbol{\theta}}(\boldsymbol{X}|C_4 = 6) + \nabla_{\mathbf{X}} \log p_{\boldsymbol{\theta}}(\boldsymbol{X}|C_6 = 11) - \nabla_{\mathbf{X}} \log p_{\boldsymbol{\theta}}(\boldsymbol{X}|C_5 = 0)\\ &- \nabla_{\mathbf{X}} \log p_{\boldsymbol{\theta}}(\boldsymbol{X}|C_5 = 1) - \nabla_{\mathbf{X}} \log p_{\boldsymbol{\theta}}(\boldsymbol{X}|C_5 = 3) - \nabla_{\mathbf{X}} \log p_{\boldsymbol{\theta}}(\boldsymbol{X})\end{aligned}$$

Similarly, for Colored MNIST, we perform two kinds of negation operations: one on digit and another on color. In Section § 2, we have shown negation on color $4 \wedge \neg[\text{Green} \vee \text{Pink}]$, along with its sampling equation. A similar logic can be followed for negation on color; an example of negation on digit is $\neg[3 \vee 4] \wedge \text{Pink}$.

For $\wedge$ and $\neg$, evaluations are strictly restricted to unseen compositions under orthogonal partial support for Shapes3D and under diagonal partial support for Colored MNIST. This approach allows us to explore how effectively the model handles logical operations through unseen image generation. Additionally, we evaluate compositions observed during training with less frequency under non-uniform support.

D.3 Training details, Architecture, and Sampling

Training Composed GLIDE & CoInD We train the diffusion model using the DDPM noise scheduler. The model architecture and hyperparameters used for all experiments are detailed in Tab. 6.

Training LACE The LACE method involves training multiple energy-based models for each attribute and sampling according to logical compositional equations. However, we use score-based models instead. We follow the architecture outlined in Tab. 6 for each attribute to train multiple score-based models. For Colored MNIST, which has two attributes, we create two models—one for each attribute—using the same architecture as other methods, effectively doubling the model size. Similarly, for Shapes3D with six attributes, we develop six models. We reduce the Block Out Channels for each attribute model to fit these into memory while keeping all other hyperparameters consistent. Since we train a single model per attribute, we do not match the joint distribution, preventing us from evaluating it and measuring the JSD.

Sampling To generate samples for a given logical composition, we sample from equations from App. D.2 using DDIM (Song et al., 2020) with 150 steps.

Hyperparameter	Colored MNIST		Shapes3D	
	CoInD & Composed GLIDE	LACE	CoInD & Composed GLIDE	LACE
Optimizer	AdamW	AdamW	AdamW	AdamW
Learning Rate	2.0×10^{-4}	2.0×10^{-4}	2.0×10^{-4}	2.0×10^{-4}
Num Training Steps	50000	100000	100000	100000
Train Noise Scheduler	DDPM	DDPM	DDPM	DDPM
Train Noise Schedule	Linear	Linear	Linear	Linear
Train Noise Steps	1000	1000	1000	1000
Sampling Noise Schedule	DDIM	DDIM	DDIM	DDIM
Sampling Steps	150	150	150	150
Model	U-Net	U-Net	U-Net	U-Net
Layers per block	2	2	2	2
Beta Schedule	Linear	Linear	Linear	Linear
Sample Size	28x3x3	28x3x3	64x3x3	64x3x3
Block Out Channels	[56,112,168]	[56,112,168]	[56,112,168,224]	**[56,112,168]**
Dropout Rate	0.1	0.1	0.1	0.1
Attention Head Dimension	8	8	8	8
Norm Num Groups	8	8	8	8
Number of Parameters	$8.2M$	$8.2M \times 2$	$17.2M$	$8.2M \times 6$

Table 6: Hyperparameters for Colored MNIST and Shapes3D used by CoInD, Composed GLIDE, and LACE

CelebA To generate CelebA images, we scale the image size to 128×128. We use the latent encoder of Stable Diffusion 3 (SD3) to encode the images to a latent space and perform diffusion in the latent space. The architecture is similar to the Colored MNIST and Shapes3D, except that Block out Channels are scaled as [224, 448, 672, 896]. We use a learning rate of 1.0×10^{-4} and train the model for 500,000 steps on one A6000 GPU.

FID Measure To evaluate both the generation quality and how well the generated samples align with the natural distribution of 'smiling male celebrities', we use the FID metric (Seitzer, 2020). Notably, we calculate the FID score specifically on the subset of 'smiling male celebrities,' as our primary objective is to assess the model's ability to generate these unseen compositions. We generate 3000 samples to evaluate FID.

T2I: Finetuning SDv1.5 We finetune SDv1.5 with the data constructed from CelebA, where the labels are converted to text. For example, a label of (male=1, smiling=1) is converted to a "photo of a smiling male celebrity."

D.4 Analytical Forms of Support Settings

The attribute space observed during training $\mathcal{C}_{\text{train}}$ covers $\mathcal{C}$ in the following sense:

Definition 1 (Support Cover)**.** *Let $\mathcal{C} = \mathcal{C}_1 \times \cdots \times \mathcal{C}_n$ be the Cartesian product of n finite sets $\mathcal{C}_1, \ldots, \mathcal{C}_n$. Consider a subset $\mathcal{C}_{train} \subset \mathcal{C}$. Let $\mathcal{C}_{train} = \{(c_{1j}, \ldots, c_{nj}) : c_{ij} \in \mathcal{C}_i, 1 \leq i \leq n, 1 \leq j \leq m\}$ and $\tilde{\mathcal{C}}_i = \{c_{ij} : 1 \leq j \leq m\}$ for $1 \leq i \leq n$. The Cartesian product of these sets is $\tilde{\mathcal{C}}_{train} = \tilde{\mathcal{C}}_1 \times \cdots \times \tilde{\mathcal{C}}_n$. We say $\mathcal{C}_{train}$ covers $\mathcal{C}$ iff $\mathcal{C} = \tilde{\mathcal{C}}_{train}$.*

Some of the support settings which cover the attribute space are given below.

Below are the analytical expressions for the densities under the various support settings that we considered in the paper. Let n_i be the number of categories for the attribute C_i. For non-uniform and diagonal partial support settings, we assume that $n_i = n_j = n, \forall i, j, i \neq j$.

- **Uniform setting:** $p(C_i = c_1) = \frac{1}{n_i}$ and $p(C_i = c_1, C_j = c_2) = p(C_i = c_1)p(C_j = c_2) = \frac{1}{n_i n_j}$.
- **Orthogonal support setting:** $p(C_i = c_1, C_j = c_2) = \begin{cases} \frac{1}{n_i + n_j - 1}, & c_1 = 0 \text{ or } c_2 = 0 \\ 0, & \text{otherwise} \end{cases}$
- **Non-uniform setting:** $p(C_i = c_1, C_j = c_2) = \begin{cases} a, & c_2 \leq c_1 \leq c_2 + 1 \\ b, & \text{otherwise} \end{cases}$, where $\frac{1}{n^2} \leq b < a \leq \frac{1}{2n-1}$.
- **Diagonal partial support setting:** $p(C_i = c_1, C_j = c_2) = \begin{cases} \frac{1}{2n-1}, & c_2 \leq c_1 \leq c_2 + 1 \\ 0, & \text{otherwise} \end{cases}$.

D.5 Datasets

Colored MNIST Dataset In Section § 1, we introduced the Colored MNIST dataset. Here, we will detail the dataset generation process. We selected 10 visually distinct colors [1], taking the value $C_2 \in [0, 9]$. The dataset is constructed by coloring the grayscale images from MNIST by converting them into three channels and applying one of the ten colors to non-zero grayscale values.

The training data is composed of three types of support:

- **Uniform Support**: A digit and a color are randomly selected to create an image.
- **Diagonal Partial Support**: A digit is selected, and during training, it is only assigned one of two colors, $C_2 \in \{d, d+1\}$, except for 9, which only takes one color. This creates a dataset where compositions observed during training are along the diagonal of the $\mathcal{C}$ space, meaning each digit is seen only with its corresponding colors.
- **Non-uniform Support**: All compositions are observed, but combining a digit and its corresponding colors occurs with a higher probability (0.5). The remaining color space is distributed evenly among other colors, resulting in approximately a 0.25 probability for each corresponding color and a 0.0625 probability for each remaining color.

Shapes3D Full support for Shapes3D consists of all samples from the dataset. For orthogonal support, we use the composition split of Shapes3D as described by Schott et al.., whose code is publicly available [2].

D.6 Conformity Score (CS)

In Section 3, we described the Conformity Score (CS) to quantify the accuracy of the generation per the prompt. To provide a formal definition

[1] `https://mokole.com/palette.html`

[2] https://github.com/bethgelab/InDomainGeneralizationBenchmark

Conformity Score (CS) To formally define CS: For a logical relation, R. This relation is defined as a boolean function over the attribute space $\mathcal{C}$, such that $R : \mathcal{C} \to \{0, 1\}$. This induces a constrained attribute space given by $\mathcal{R} = \{(c_1, \dots, c_n) \mid R(c_1, \dots, c_n) = 1\} \subseteq \mathcal{C}$. The CS is defined as:

$$\text{CS}(R, \theta) := \mathbb{E}_{C \sim p(C)} \mathbb{E}_{U \sim p(U)} \left[\mathbb{1}_{\mathcal{R}_C} \left((\phi_{C_i}(g_\theta(R(C), U)))_{i=1}^{n} \right) \right] \tag{30}$$

where $R(C)$ can represent various logical operations such as $\wedge$, $\neg$, and $\vee$ on the attribute space $\mathcal{C}$. Here, $g_\theta(R(C), U)$ denotes a generative model parameterized by θ, which samples according to the logical relations specified above. The variable U represents exogenous noise in the diffusion model. The functions ϕ_{C_i} are attribute-specific classifiers that infer attributes from the generated images. The term $\mathbb{1}_{\mathcal{R}_C}$, is an indicator function, equals 1 if the inferred attributes $(\phi_{C_i}(g_\theta(R(C), U)))_{i=1}^{n} \subseteq \mathcal{R}_C$.

To measure the CS, we train a single ResNet-18 (He et al., 2016) classifier with multiple classification heads, one corresponding to each attribute, and trained on the full support. This classifier estimates the attributes in the generated image, $\mathbf{x}$, and extracts these attributes as $\phi(\mathbf{x}) = [\hat{c_1}, \dots, \hat{c_n}]$. These attributes are matched against the input prompt that generated the image to obtain accuracy.

To explain further, for example, if the prompt is to generate "$4 \wedge \neg$[Green $\vee$ Pink]", the generated sample will have a CS of 1 if $\hat{c_1} = 4$ and $\hat{c_2} \notin \{\text{Green}, \text{Pink}\}$. We average this across all the prompts in the test set, which determines the CS for a given task.

The effectiveness of the classifier in predicting the attributes is reported in Table 8.

Feature	Attributes	Possible Values	Accuracy
C_1	Digit	0-9	98.93
C_2	color	10 values	100

(a) Colored MNIST Dataset

Feature	Attributes	Possible Values	Accuracy
C_1	Gender	{0,1}	98.2
C_2	Smile	{0,1}	92.1

(b) CelebA Dataset

Feature	Attributes	Possible Values	Accuracy
C_1	floor hue	10 values in [0, 1]	100
C_2	wall hue	10 values in [0, 1]	100
C_3	object hue	10 values in [0, 1]	100
C_4	scale	8 values in [0, 1]	100
C_5	shape	4 values in [0-3]	100
C_6	orientation	15 values in [-30, 30]	100

(c) Shapes3D Dataset

Figure 8: Independent attribute, their possible values, and the classifier accuracy in estimating them for different datasets

D.7 Computing JSD

We are interested in understanding the causal structure learned by diffusion models. Specifically, we aim to determine whether the learned model captures the conditional independence between attributes, allowing them to vary independently. This raises the question: *Do diffusion models learn the conditional independence between attributes?* The conditional independence is defined by:

$$p_{\boldsymbol{\theta}}(C_i, C_j \mid \boldsymbol{X}) = p_{\boldsymbol{\theta}}(C_i \mid \boldsymbol{X}) p_{\boldsymbol{\theta}}(C_j \mid \boldsymbol{X}) \tag{31}$$

We aim to measure the violation of this equality using the Jensen-Shannon divergence (JSD) to quantify the divergence between two probability distributions:

$$\text{JSD} = \mathbb{E}_{p_{\text{data}}} \left[D_{\text{JS}} \left(p_{\boldsymbol{\theta}}(C \mid \boldsymbol{X}) \,||\, p_{\boldsymbol{\theta}}(C_i \mid \boldsymbol{X}) p_{\boldsymbol{\theta}}(C_j \mid \boldsymbol{X}) \right) \right] \tag{32}$$

The joint distribution, $p_{\boldsymbol{\theta}}(C_i, C_j \mid \boldsymbol{X})$, and the marginal distributions, $p_{\boldsymbol{\theta}}(C_i \mid \boldsymbol{X})$ and $p_{\boldsymbol{\theta}}(C_j \mid \boldsymbol{X})$, are evaluated at all possible values that C_i and C_j can take to obtain the probability mass function (pmf). The probability for each value is calculated using Equation Eq. (14) for the joint distribution and Equation Eq. (13) for the marginals.

Practical Implementation For the diffusion model with multiple attributes, the violation in conditional *mutual* independence should be calculated using all subset distributions. However, we focus on pairwise independence. We further approximate this in our experiments by computing JSD between the first two attributes, C_1 and C_2. We have observed that computing JSD between any attribute pair does not change our examples' conclusion.

D.8 Measuring Diversity in Attributes

To achieve explicit control over certain attributes during the generation process, these attributes must vary independently. Therefore, an ideal generative model must be able to produce samples where all except the controlled attributes take diverse values. This diversity can be measured by the entropy of the uncontrolled attributes in the generated samples, where higher entropy suggests greater diversity. Therefore, the accurate generation of controlled and diverse uncontrolled attributes indicates that the model has successfully learned the correct marginal likelihood of the controlled attributes.

For example, consider the generation of colored MNIST digits. In this case, controllability means that the model has learned that digit and color attributes are independent. When prompted to generate a specific digit (controlled attribute), the model should generate this digit in all possible colors (uncontrolled attribute) with equal likelihood, implying maximum entropy for the color attribute and diverse generation. We measure this entropy by generating samples $x^i \sim p_\theta(X \mid c_1 = 4)$ and passing them through a near-perfect classifier to obtain the color predictions $p(\hat{C_2}) = p(\phi_2(x^i))$. The diversity is then quantified as: $H = \mathbb{E}_{\hat{c_2} \sim p(\hat{C_2})} \left[\log_2 p(\hat{c_2})\right]$

Ensuring diversity through explicit control has applications in bias detection and mitigation in generative models. For example, a biased model may generate images of predominantly male doctors when asked to generate images of "doctors". Ensuring diversity in uncontrolled attributes like gender or race can limit such biases.

E CoInD for Face Image Generation

In § 5, we demonstrated that CoInD outperforms baseline methods on the unseen logical compositionality task using synthetic datasets. In App. E.1, we showcase the success of CoInD in generating face images from the CelebA dataset (Liu et al., 2015), where CoInD demonstrates superior control over attributes compared to the baseline. CoInD also allows us to adjust the strength of various attributes and thus provides more fine-grained control over the compositional attributes, as shown in App. E.2. Finally, in App. E.3, we extend CoInD to text-to-image (T2I) models widely used in practice to generate face images by providing the desired attributes as logical expressions of text prompts.

Problem Setup We choose the CelebA dataset to evaluate CoInD's ability to generate real-world images. We choose the binary attributes "smiling" and "gender" as the attributes we wish to control. During training, all combinations of these attributes except gender = "male" and smiling = "true" are observed, similar to the orthogonal support. During inference, the model is tasked to generate images with the attribute combination gender = "male" and smiling = "true", which was not observed during training.

Metrics Similar to the experiments on the synthetic image datasets in § 5, we assess the accuracy of the generation w.r.t. the input desired attribute combination CS (conformity score). We also measure the violation of the learned conditional independence using JSD. In addition to CS, we compute FID (Fréchet inception distance) between the generated images and the real samples in the CelebA dataset where gender = "male" and smiling = "true". A lower FID implies that the distribution of generated samples is closer to the real distribution of the images in the validation dataset.

E.1 CoInD can successfully generate real-world face images

Tab. 3 shows the quantitative results of CoInD and Composed GLIDE trained from scratch in the tasks of joint sampling and $\wedge$ composition. Similar to our observations from previous experiments, CoInD achieves better CS in both tasks by learning accurate marginals as demonstrated by lower JSD. When sampled from the joint likelihood, CoInD achieves a nearly $4\times$ improvement in CS over the baseline, while it achieves $> 10\%$ improvement in CS over the baseline, for $\wedge$ compositionality.

E.2 CoInD provides fine-grained control over attributes

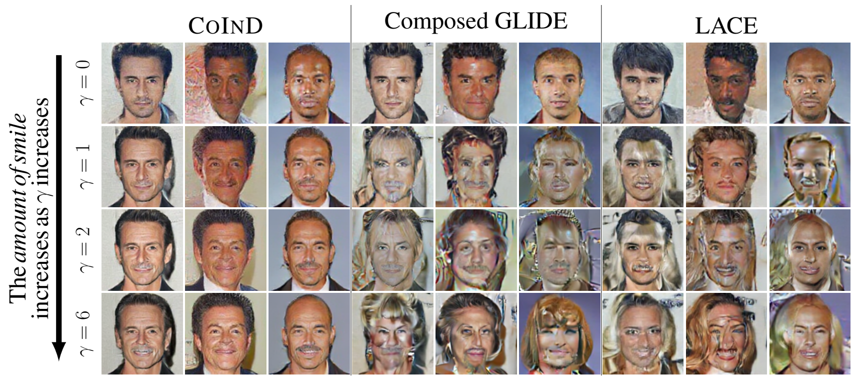

Figure 9: By adjusting γ, CoInD allows us to the vary the *amount of "smile"* in the generated images. However, Composed GLIDE associates the smile attribute with the gender attribute due to their association in the training data. Hence, the images generated by Composed GLIDE contain gender-specific attributes such as long hair and earrings.

So far, we studied the capabilities of CoInD to dictate the presence and absence of attributes in the task of controllable image generation. However, there are applications where we desire fine-grained control over the attributes. Specifically, we may want to control the *amount of each attribute* in the generated sample. We can mathematically formulate this task by revisiting the formulation of logical expressions of attributes in terms of the score functions of marginal likelihood. As an example, the $\wedge$ operation can be written as,

$$\nabla_{\boldsymbol{X}} \log p_{\boldsymbol{\theta}}(\boldsymbol{X} \mid C_1 \wedge C_2) = \nabla_{\boldsymbol{X}} \log p_{\boldsymbol{\theta}}(\boldsymbol{X} \mid C_1) + \nabla_{\boldsymbol{X}} \log p_{\boldsymbol{\theta}}(\boldsymbol{X} \mid C_2) - \nabla_{\boldsymbol{X}} \log p_{\boldsymbol{\theta}}(\boldsymbol{X})$$

Here, to adjust the amount of attribute added to the generated sample, we can weigh the score functions using some scalar γ, as follows,

$$\nabla_{\boldsymbol{X}} \log p_{\boldsymbol{\theta}}(\boldsymbol{X} \mid C_1) + \gamma \nabla_{\boldsymbol{X}} \log p_{\boldsymbol{\theta}}(\boldsymbol{X} \mid C_2) - \gamma \nabla_{\boldsymbol{X}} \log p_{\boldsymbol{\theta}}(\boldsymbol{X}) \tag{33}$$

where γ controls for the amount of C_2 attribute.

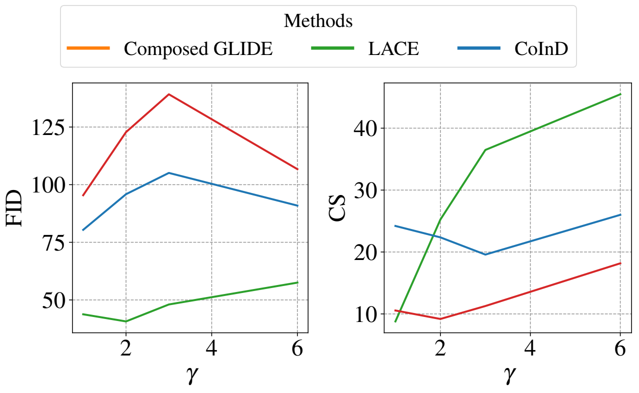

(a) Variation of FID with γ (b) Variation of CS with γ

Figure 10: **Effect of γ on FID and CS:** Varying the amount of smile in a generated image through γ does not affect the FID of CoInD. However, the smiles in the generated images become more apparent, leading to easier detection by the smile classifier and improved CS.

Fig. 9 shows the effect of increasing γ to adjust the amount of smiling in the generated image. Ideally, we expect increasing γ to increase the amount of smiling without affecting the gender attribute. When $\gamma = 0$ (top row), both CoInD and Composed GLIDE generate images of men who are not smiling. As γ increases, we notice that the samples generated by CoInD show an increase in the amount of smiling, going from a short smile to a wider smile to one where teeth are visible. Note that the training dataset did not include any images of smiling men or fine-grained annotations for the amount of smiling in each image. This conclusion is strengthened by Fig. 10b that shows an increase in CS when γ increases. CS increases when it is easier for the smile classifier to detect the smile. CoInD provides this fine-grained control over the smiling attribute without any effect on the realism of the images, as shown by the minimal changes in FID in Fig. 10a.

In contrast, the images generated by Composed GLIDE show an increase in the amount of smiling while adding gender-specific attributes such as long hair and makeup. We conclude that, by strictly enforcing a conditional independence loss between the attributes, CoInD provides fine-grained control over the attributes, allowing us to adjust the intensity of the attribute in the image without additional training. As shown in Tab. 3, CoInD outperforms the baselines for generating unseen compositions. Tuning γ further improves the generation.

E.3 Finetuning T2I models with CoInD improves logical compositionality

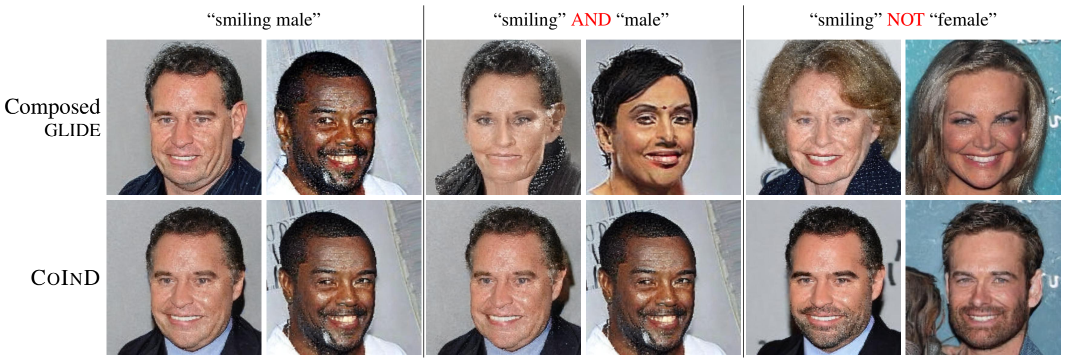

Figure 11: Samples generated after fine-tuning SDv1.5 on CelebA. The first row shows images generated by SDv1.5 fine-tuned on CelebA, while the second row shows images generated by SDv1.5 fine-tuned with CoInD. Columns indicate samples generated from the respective prompts indicated above.

We proposed CoInD to improve control over the attributes in an image through logical expressions of these attributes. Since larger pre-trained diffusion models such as Stable Diffusion (Rombach et al., 2022) have become more accessible, we seek to incorporate the benefits of CoInD in these models. This section shows that text-to-image (T2I) models can be fine-tuned to generate images using logical expressions of text prompts. Specifically, we use Stable Diffusion v1.5 (SDv1.5) to generate face images from the CelebA dataset where smiling and gender attributes can be controlled. We consider both joint and marginal sampling, similar to our case study in § 3. For joint sampling, we provide SDv1.5 with the prompt "photo of a smiling male celebrity". In the marginal sampling, we provide the values for smiling and gender attributes using separate prompts – "Photo of a smiling celebrity" $\wedge$ "Photo of a male celebrity". Then, we sample from these marginal likelihoods resulting from these prompts following Eq. (1). To evaluate $\neg$ capabilities, we use the prompts "Photo of a smiling celebrity" $\neg$ "Photo of a female celebrity" and follow Eq. (2).

Support	Method	JSD ↓	Joint		∧ Composition		¬ Composition	
			CS ↑	FID ↓	CS ↑	FID ↓	CS ↑	FID ↓
Orthogonal	Composed GLIDE	0.57	56.57	58.31	14.19	73.53	11.02	115.95
	CoInD ($\lambda = 1.0$)	**0.37**	**58.57**	**58.19**	**49.15**	**61.16**	**18.80**	**86.31**

Table 7: **Results on SDv1.5 fine-tuning.** CoInD outperforms the baseline on all the metrics.

Discussion

1. In Tab. 7, CoInD improves performance across all metrics – achieving $3.46\times$ and $2\times$ improvement in CS over Composed GLIDE in $\wedge$ and $\neg$ composition tasks. The images generated by CoInD have better FID than those from the baseline.

2. Visual inspection of the generated samples for the same random seed provides insights into how Composed GLIDE and CoInD perceive the prompts. Images in columns 1, 3, and 5 of Fig. 11 were generated with the same random seed. Similarly, those in columns 2 and 4 share the random seed. We note the following observations:

   – Both Composed GLIDE and CoInD generated images with the desired attributes when sampled from the joint likelihood using "photo of a smiling male celebrity". The images generated by these models from the same random seed were also visually similar. This shows that both models can aptly set attributes in the generated images and have identical stochastic profiles, leading to unspecified attributes that assume similar values.

   – When the attributes were passed as the $\wedge$ expression "smiling" $\wedge$ "male", CoInD generated images that were visually similar to those with matching random seeds generated from joint sampling. This implies that CoInD learned accurate marginals that help it to correctly model the joint likelihood.

   – When tasked with generating images for "smiling" $\wedge$ "male", Composed GLIDE generated images of smiling persons with gender-specific attributes such as thinner eyebrows, commonly seen in photos of female celebrities. These gender-specific features increase when the task is to generate images of "smiling" $\neg$ "female". In contrast, CoInD generates images of smiling celebrities while adding attributes such as a beard. Thus, we conclude that CoInD offers better control over the desired attributes without affecting correlated attributes.

F Discussion on CoInD

F.1 Compositional vs Monolithic models

Our findings echo the prior observations (Du & Kaelbling, 2024) that composite models consisting of separate diffusion models trained on individual factors (e.g., LACE) demonstrate better $\wedge$ compositionality under partial support than sampling from factorized distributions learned by monolithic models (e.g., Composed GLIDE). However, we found that monolithic models can be significantly improved by enforcing the conditional independence constraints necessary for enabling logical compositionality. For instance, CoInD achieved a $2.4\times$ better CS on Colored MNIST with diagonal partial support and a $1.4\times$ improvement on orthogonal partial support on Shapes3D compared to LACE.

F.2 Connection to compositional generation from first principles

Compositional generation from first principles Wiedemer et al. (2024) have shown that restricting the function to a certain compositional form will perform better than a single large model. In this section, we show that, by enforcing conditional independence, we restrict the function to encourage compositionality.

Let $c_1, c_2, \ldots, c_n$ be independent components such that $c_1, c_2, \ldots, c_n \in \mathbb{R}$. Consider an injective function $f : \mathbb{R}^n \to \mathbb{R}^d$ defined by $f(c) = x$. If the components, c are conditionally independent given x the cumulative functions, F must satisfy the following constraint:

$$F_{C_i, C_j, \ldots, C_n | X=x}(c_i, c_j, \ldots, c_n) = \prod_i F_{C_i|X=x}(c_i) \tag{34}$$

$F^{-1}_{C_i,C_j,\ldots,C_n|X=x}(x) = \inf\{c_i, c_j, \ldots, c_n \mid F(c_i, c_j, \ldots, c_n) \geq x\}$, where $F^{-1}_{c_i,c_j,\ldots,C_n|X=x}$ is a generalized inverse distribution function.

$$\begin{aligned} f(c_i, c_j, \ldots, c_n) &= (f \circ F^{-1}_{c_i,c_j,\ldots,C_n|X=x})(\prod_i F_{C_i|X=x}(c_i)) \\ &= (f \circ F^{-1}_{c_i,c_j,\ldots,C_n|X=x} \circ e)(\sum_i \log F_{C_i|X=x}(c_i)) \\ &= g(\sum_i \phi_i(c_i)) \end{aligned}$$

Therefore, we are restricting f to take a certain functional form. However, it is difficult to show that the data generating process, f, meets the rank condition on the Jacobian for the sufficient support assumption Wiedemer et al. (2024), which is also the limitation discussed in their approach. Therefore, we cannot provide guarantees. However, this section provides a functional perspective of CoInD.

F.3 Limitations

This paper considered compositions of a closed set of attributes. As such, CoInD requires pre-defined attributes and access to data labeled with the corresponding attributes. Moreover, CoInD must be enforced during training, which requires retraining the model whenever the attribute space changes to include additional values. Instead, state-of-the-art generative models seek to operate without pre-defined attributes or labeled data and generate open-set compositions. Despite the seemingly restricted setting of our work, our findings provide valuable insights into a critical limitation of current generative models, namely their failure to generalize for unseen compositions, by identifying the source of this limitation and proposing an effective solution to mitigate it.

G Additional Results and Discussion on CoInD

G.1 Learning under non-uniform $p(C_i)$

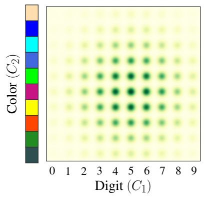

(a) Gaussian support

Method	JSD ↓	∧ (CS) ↑	¬ Color (CS)↑	¬ Digit (CS) ↑
LACE	-	89.22	58.59	57.81
Composed GLIDE	0.27	91.74	88.91	78.39
CoInD ($\lambda = 1.0$)	**0.16**	**99.61**	**98.51**	**83.03**

(b) Quantitative results for Gaussian support

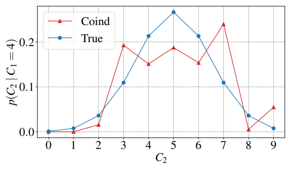

(c) $p(C_2 \mid C_1 = 4)$ vs $p_{\boldsymbol{\theta}}(C_2 \mid C_1 = 4)$

Figure 12: **Results on Gaussian support:** When the independent attributes have non-uniform categorical distributions, the joint distribution of attribute combinations is not uniform. Even in this case, CoInD learns $p_{\boldsymbol{\theta}}(C_i \mid C_j)$ accurately.

In our experiments, we considered the uniform support setting as an example where the attribute variables are independent of each other in the training data, i.e., $C_1 \perp\!\!\!\perp C_2 \mid \boldsymbol{X}$ during training. However, uniform support is not the only scenario that can arise from independent attribute variables. In this section, we show that CoInD can learn accurate marginals irrespective of the distribution of C_i.

We designed an experiment using the Colored MNIST images where the attributes C_1 and C_2 assume values from a non-uniform categorical distribution that resembles a discrete Gaussian distribution. The resulting joint distribution of the attributes, which we refer to as *Gaussian support*, is illustrated in Fig. 12a. We trained CoInD and baselines on this dataset and evaluated on $\wedge$ and $\neg$ compositionality tasks. Apart from comparing the CS of baselines and CoInD on these compositionality tasks, we also evaluate if CoInD accurately learns $p(C_i)$ by comparing the learned

$p_{\boldsymbol{\theta}}(C_i \mid C_j)$ against the true $p(C_i \mid C_j)$. Intuitively, this verifies if CoInD generates images with uncontrolled attributes matching their distribution in the training dataset.

Fig. 12b quantitatively compares CoInD against Composed GLIDE on CS in both $\wedge$ and $\neg$ compositionality tasks. Like our previous experiments, CoInD outperforms Composed GLIDE w.r.t. CS in all tasks. In Fig. 12c, we verify if CoInD has learned $p_{\boldsymbol{\theta}}(C_2 \mid C_1)$ accurately by comparing it against the true distribution $p(C_2 \mid C_1)$. $p_{\boldsymbol{\theta}}(C_2 \mid C_1 = c^*) = p_{\boldsymbol{\phi}}(C_2 \mid X)p_{\theta}(X \mid C_1 = c^*)$ is obtained as the histogram density of the attributes that appear in the generated images when $C_1 = c^*$. We observe that the learned distribution $p_{\boldsymbol{\theta}}(C_2 \mid C_1 = 4)$ is close to the true distribution, forming a bell shape.

G.2 Conformity score for each attribute combination

In all our experiments, we report CS as the primary metric to evaluate if the generative model produced images with accurate attributes. However, CS is the average accuracy across all unseen attribute combinations. Not all attribute combinations may be generated with equal accuracy. For instance, Fig. 13 shows the CS for each attribute combination in the $\wedge$ compositionality task in Colored MNIST image generation with partial support setting (row 10 in Fig. 3a). As a reminder, CoInD achieved 55% CS on unseen attribute combinations in this task. We can see that CoInD can successfully generate all seen attribute combinations that appear on the diagonal. Some unseen attribute combinations achieve $> 90\%$ CS, while others have nearly 0% CS.

We do not observe the model struggling to generate images with any specific attribute or digit, although some colors have a generally lower CS than others. For example, colors 2 and 3 have zero CS with more digits than others. On the other hand, colors 4, 5, and 6 have high CS with all digits. We hypothesize that this disparity in CS could depend on the nature of attributes and the similarity between the values they can take.

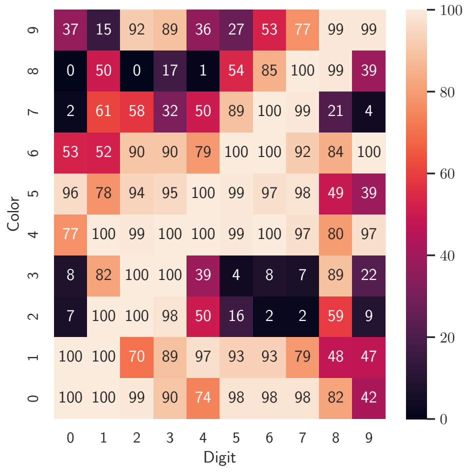

Figure 13: Heatmap showing CS for each attribute combination in the $\wedge$ compositionality task in Colored MNIST generation with partial support (row 10 in Fig. 3a)

G.3 Failure examples of CoInD

Here, we examine some samples generated by CoInD where it failed to include the desired attributes. We show these failure cases from each dataset, i.e., Colored MNIST, Shapes3d, and CelebA datasets. Samples from Colored MNIST and Shapes3d datasets are taken from the partial support setting, while the ones from the CelebA dataset are taken from the orthogonal support setting. Fig. 14a shows some failure samples from the Colored MNIST dataset. The images in the first row contain digits with colors leaking from the nearby seen attribute combination. Those in the second row correspond to $\neg$ approximation and have wrong attributes due to the approximation in the probabilistic formulation in Eq. (2). Some images, like those in the third row, are unrealistic, although they may contain the desired attributes. We observe similar failures in Shapes3d samples shown in Fig. 14b where the CoInD deviates from the desired compositions (column 1). Some failed samples from the CelebA dataset are shown in Fig. 14c. The samples correspond to the task of "smile" $\wedge$ "male". In the top image, it is hard to distinguish if the subject is smiling or laughing. In some samples, we observed only a weak or soft smile. This could be because a smile is difficult to control due to its limited spatial presence in an image.

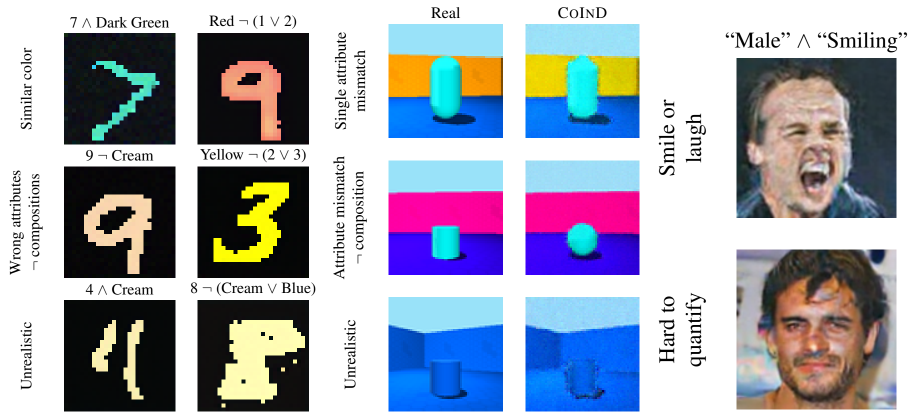

(a) Failure samples from Colored MNIST dataset (b) Failure samples from Shapes3d dataset (c) Failure samples from CelebA dataset

Figure 14: Some samples generated by CoInD where it could not enforce the desired attributes.

Support	Configuration	CS
Uniform	Vanilla	100
Uniform	CoInD($\lambda = 1$)	100
Non-uniform	Vanilla	100
Non-uniform	CoInD($\lambda = 1$)	100
Diagonal partial	Vanilla	65.27
Diagonal partial	CoInD($\lambda = 1$)	73.35

(a) Colored MNIST

Support	Configuration	R^2	CS
Uniform	Vanilla	0.99	100
Uniform	CoInD($\lambda = 1$)	0.99	100
Orthogonal partial	Vanilla	0.97	95.88
Orthogonal partial	CoInD($\lambda = 1$)	0.99	99.57

(b) Shapes3D

Table 8: Overall Performance Metrics for Conditional generation

G.4 CoInD also improves conditional generation

Given an ordered n-tuple from the attribute space not observed during training, can CoInD generate images corresponding to this sampled from joint distribution, $P_\theta(X|C)$? To answer this question, we train CoInD and the baselines on Colored MNIST and Shapes3d datasets. Tab. 8 shows the results. As expected, the vanilla model, under full support, generates samples corresponding to the joint distribution. However, as demonstrated in § 3, models trained on partial support fail to generate samples for unseen attribute compositions. In addition to the improved performance on logical compositionality, enforcing conditional independence explicitly improves conditional generation as well and produces better results on partial support compared to vanilla diffusion models for both Colored MNIST and Shapes3D datasets.

H 2D Gaussian: Workings of CoInD in closed form

The underlying data is generated by two independent attributes, C_1 and C_2. The observed variable $\mathbf{X}$ is defined as:

$$\mathbf{X} = f(\mathbf{C}_1) + f(\mathbf{C}_2) \tag{35}$$

where $f(c_i) = c_i + \sigma\epsilon$, and $\epsilon \sim \mathcal{N}(0, I)$ represents Gaussian noise. For simplicity, C_1 and C_2 are binary variables taking values in $\{-1, +1\}$. The function $f(C_1)$ results in a mixture of Gaussians with means $[-1 \quad 0]$ and $[+1 \quad 0]$. These are represented along the x-axis in Figure 15a. Similarly, $f(C_2)$ produces a mixture of Gaussians with means:$[0 \quad -1]$ and $[0 \quad +1]$. These are displayed along the y-axis in Figure 15a. The combination of C_1 and C_2 independently generates as Eq. (35) This results in a two-dimensional Gaussian mixture, as illustrated in Figure 15. We consider orthogonal support, where attribute combinations of $(C_1, C_2) \in \{(-1, -1), (-1, +1), (+1, -1)\}$, and the model is tasked to generate unseen combination of $(+1, +1)$. Also as a reminder that assumptions mentioned in § 2 are satisfied. (1) C_1, C_2 independently generate $\boldsymbol{X}$, and (2) all possibles values for

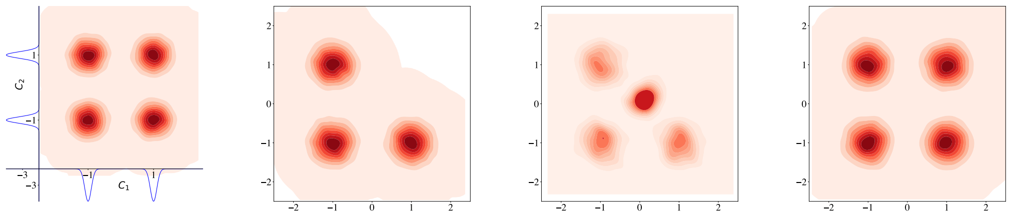
(a) True underlying data distribution (b) Training data Orthogonal Support (c) Conditional distribution learned by vanilla diffusion objective (d) Conditional distribution learned by CoInD

Figure 15: CoInD respects underlying independence conditions thereby generating true data distribution (d).

every attribute are present at-least observed during training. Let score is given by $s_{+1,+1}$ represents $\nabla_{\mathbf{X}} \log p(X \mid C_1 = 1, C_2 = 1)$ and likewise $s_{1,\varnothing}$ represents $\nabla_{\mathbf{X}} \log p(X \mid C_1)$ To sample for the unseen compositions of (1,1) we use Eq. (1) to

$$s_{1,1}(x) = s_{1,\varnothing}(x) + s_{\varnothing,1}(x) - s_{\varnothing,\varnothing}(x) \tag{36}$$

Training diffusion model (score) objective involves computing score functions from the training data, which will give us the following terms in closed form. For example $s_{1,\varnothing}(x)$ is training using only $+1, -1$ combinations present during training. which is nothing but a gaussian at $+1, -1$ and the score of the gaussian is given in closed form.

$$s_{1,\varnothing}(x) = \frac{\mu_{1,-1} - x}{\sigma^2}$$
$$s_{\varnothing,1}(x) = \frac{\mu_{1,-1} - x}{\sigma^2}$$

$s_{\varnothing,\varnothing}(x)$ is a mixture of gaussian with means around 3 Gaussians present during training. The score of the mixture gaussian as:

$$s_{\varnothing,\varnothing}(x) = \frac{\sum_i \mathcal{N}(x; \mu_i, \sigma^2 I)\left[\frac{\mu_i - x}{\sigma^2}\right]}{\sum_i \mathcal{N}(x; \mu_i, \sigma^2 I)}$$

Now leveraging Langevin dynamics Eq. (9) will generate the Fig. 15c as the distribution of $P(X \mid C_1 = +1, C_2 = +1)$ is incorrect (strong red blob between the $(+1, -1), (-1, +1)$ instead of gaussian at (+1,+1)). This is due to incorect modelling of the distributions $s_{1,\varnothing}(x), s_{\varnothing,1}(x), s_{\varnothing,\varnothing}(x)$. However, CoInD does not explicitly model $s_{1,\varnothing}$, instead learn joint $s_{-1,-1}(x), s_{+1,-1}(x), s_{-1,+1}(x)$ as Gaussians and then combine them using pairwise conditional independence conditions given as:

$$\begin{aligned}
s_{-1,-1}(x) &= s_{+1,\varnothing}(x) + s_{\varnothing,+1}(x) - s_{\varnothing,\varnothing}(x) \\
s_{+1,-1}(x) &= s_{+1,\varnothing}(x) + s_{\varnothing,-1}(x) - s_{\varnothing,\varnothing}(x) \\
s_{-1,+1}(x) &= s_{-1,\varnothing}(x) + s_{\varnothing,+1}(x) - s_{\varnothing,\varnothing}(x) \\
s_{+1,1}(x) &= s_{+1,\varnothing}(x) + s_{\varnothing,+1}(x) - s_{\varnothing,\varnothing}(x) \\
&= s_{+1,-1}(x) + s_{-1,+1}(x) - s_{-1,-1}(x) \\
&= \frac{[\mu_{+1,-1} + \mu_{+1,-1} - \mu_{-1,-1}] - x}{\sigma^2}
\end{aligned}$$

This shows the workings of CoInD and also demonstrates that conditional independence constraints are necessary to learn the underlying distribution and alos with these constraints, diffusion models generate incorrect interpolation for unseen data distributions as shown in Fig. 15c.

I Extension to Gaussian source flow models

Diffusion models can be viewed as a specific case of flow-based models where: (1) the source distribution is Gaussian, and (2) the forward process follows a predetermined noise schedule.(Lipman et al., 2024). Can we reformulate COIND in terms of velocity rather than score, thereby generalizing it to accommodate arbitrary source distributions and schedules? When the source distribution is gaussian, score and velocity are related by affine transformation as detailed in Tab. 1 of (Lipman et al., 2024).

$$s^t_\theta(x, C_1, C_2) = a_t x + b_t u^t_\theta(x, C_1, C_2) \tag{37}$$

replacing $s^t_\theta(\cdot)$ into Eq. (28)

$$\begin{aligned}\mathcal{L}_{\text{CI}} &= \mathbb{E}_{p(\boldsymbol{X},C),t\sim U[0,1]}\mathbb{E}_{j,k}\|s^t_{\boldsymbol{\theta}}(x, C_j, C_k) - s^t_{\boldsymbol{\theta}}(x, C_j) - s^t_{\boldsymbol{\theta}}(x, C_k) + s^t_{\boldsymbol{\theta}}(x)\|^2_2 \\ &= \mathbb{E}_{p(\boldsymbol{X},C),t\sim U[0,1]}\mathbb{E}_{j,k}\left[b^2_t\|u^t_{\boldsymbol{\theta}}(x, C_j, C_k) - s^t_{\boldsymbol{\theta}}(x, C_j) - u^t_{\boldsymbol{\theta}}(x, C_k) + u^t_{\boldsymbol{\theta}}(x)\|^2_2\right]\end{aligned}$$

However we can ignore b^2_t, weighting for the time step t.

$$\mathcal{L}_{\text{CI}} = \mathbb{E}_{p(\boldsymbol{X},C),t\sim U[0,1]}\mathbb{E}_{j,k}\left[\|u^t_{\boldsymbol{\theta}}(x, C_j, C_k) - u^t_{\boldsymbol{\theta}}(x, C_j) - u^t_{\boldsymbol{\theta}}(x, C_k) + u^t_{\boldsymbol{\theta}}(x)\|^2_2\right] \tag{38}$$

Therefore, if the source distribution is gaussian and for any arbitrary noise schedule, constraint in score translates directly to velocity constraint as given as Eq. (38).